

①

*Optically Induced Metastable States  
in  
Amorphous  $As_2S_3$*

非晶質  $As_2S_3$  における光誘起準安定状態

**Tetsuya Tada**

多田 哲也

*Department of Physics*

*Faculty of Science*

*University of Tokyo*

*November, 1990*

①

Acknowledgements

**Optically Induced Metastable States  
in  
Amorphous  $As_2S_3$**

非晶質  $As_2S_3$  における光誘起準安定状態

**Tetsuya Tada**

多田 哲也

**Department of Physics**

**Faculty of Science**

**University of Tokyo**

**November, 1990**

## Acknowledgements

I am indebted to Professor Toshiyuki Ninomiya, who has introduced me into the physics in amorphous semiconductors, for continual guidance, encouragement, and supervising the present thesis patiently. I wish to express my sincere gratitude to Professor Kazuro Murayama for his guidance in my postgraduate school days. I am grateful to Dr. Hironari Matsuda for his guidance of the ODMR technique.

I am pleased to acknowledge fruitful discussion with Dr. Kaoru Kimura, Mr. Masanori Iwahashi, Dr. Atsuko Yamaguchi, Mr. A. Atsushi Yamaguchi, Mr. Hidefumi Akiyama, and all of the members of the research group under Professor T. Ninomiya. My thanks are extended to Professor Keiji Tanaka and Professor K. Shimakawa for stimulative discussion. I am also grateful to Dr. David Y. K. Ko for the critical reading of this thesis.

I also wish to thank Professor N. Shima, Dr. S. Tsuneyuki, Mr. S. Koshihara, Professor K. Morigaki, and Professor Y. Tokura and the members of their research groups for encouragements. I also thank SONY corporation for the use of the high power laser diode.

Last but not at least, I wish to thank my parents and old friends for many years of encouragements.

# Contents

<b>1. Introduction</b>	<b>1</b>
<b>2. A Brief Summary of The Optical Phenomena in Chalcogenide Glasses</b>	<b>4</b>
2.1 Absorption Spectra	4
2.2 Photoluminescence	7
2.2.1 The Photoluminescence Excitation Spectra	11
2.2.2 The Temperature Dependence of the PL Intensity	14
2.2.3 Time Resolved Photoluminescence	15
2.2.4 ODMR Measurements	16
2.3 Optically Induced Phenomena	
2.3.1 Optically Induced ESR and Below-Gap Absorption band	22
2.3.2 Photoluminescence Fatigue	24
2.4 Structure of Crystalline $As_2S_3$	27
<b>3. Experimental</b>	<b>30</b>
3.1 Sample Preparation	30
3.2 Photoluminescence Measurement	30
3.3 Optically Detected Magnetic Resonance	33
<b>4. Results</b>	<b>35</b>
4.1 PL1 and PL2	35
4.2 Excitation Energy Dependence of PL	37
4.3 Annealing Properties of PL centers	37
4.4 Compositional Dependence of PL	46

4.5 Thermal Quenching of PL	46
4.6 Excitation Intensity Dependence	54
4.7 PL1 fatigue and PL2 Growth	54
4.8 Time Resolved Measurements	57
4.8.1 Excitation energy dependence of PL Decay	57
4.8.2 Temperature Dependence of PL2 Decay	63
4.8.3 Compositional Dependence of Decay	66
4.9 ODMR Spectra	68
4.10 Photoluminescence in Crystalline $As_2S_3$	68
4.11 Summary of Experimental Results	71
<b>5. Discussion</b>	<b>73</b>
5.1 Photoluminescence Fatigue	73
5.1.1 Irradiation Time Dependence	75
5.2 The PL2 Centers	76
5.2.1 The Energy Levels of PL2 Centers	80
5.2.2 The Temporal Behavior of PL2	83
5.3 Microscopic Model of The Optically Induced Defects	88
5.3.1 PL Centers in Crystalline Chalcogenides	88
5.3.2 PL Fatigue	90
5.3.3 PL2 centers	94
<b>6. Summary and Concluding Remarks</b>	<b>96</b>
<b>Appendix The Principle of ODMR</b>	<b>97</b>
<b>References</b>	<b>100</b>

## Chapter 1

### Introduction

Man has been using glasses since the ancient Egyptian age, or probably even before. It has a much longer history than that of the use of synthetic crystals, which only began at the beginning of this century. However, from the viewpoint of the solid state physics, we must say that one still does not understand the properties of glasses satisfactorily. For amorphous materials, broad and featureless signals are always observed in any measurement, which prevent us to obtain the detailed information on their physical and chemical properties. Furthermore theoretical works are difficult to develop because of the lack of symmetry.

Since the discovery of electrical switching phenomena in the films of chalcogenide glasses [Ovshinsky 1968], glassy or amorphous semiconductors have been energetically studied. Many photoinduced phenomena have been discovered, and they have become one of the most important problems in amorphous semiconductor. In chalcogenide glasses, for example, photostructural change accompanying photodarkening, optically induced ESR, optically induced below-gap absorption, and the photoluminescence (PL) fatigue were all discovered in 1970's. These phenomena are induced by the irradiation of the light whose energy is greater than the band-gap energy (the above-gap light) at low temperature. The photostructural change and the photodarkening are stable at room temperature and can be annealed out at the glass transition temperature. However the optically induced ESR, the below-gap absorption, and the PL fatigue are stable only at low temperatures and are annealed out at room temperature. In hydrogenated amorphous silicon (a-Si:H), the Staebler-Wronski effect is a famous photoinduced phenomenon, where photoconductivity and dark

conductivity are reduced with prolonged optical exposure.

The metastability of the photoinduced phenomena originates from the non-rigidity of the amorphous structures where local minima of energy are present for several configurations. Above-gap irradiation and thermal treatments induce the transitions between the local minima. Chalcogenide glasses, which contain dihedral coordinated configurations, are more flexible than tetrahedral amorphous semiconductors such as a-Si:H. Thus, the chalcogenide glasses exhibit more photoinduced phenomena, compared to tetrahedrally bonded semiconductors.

Chalcogenide glasses have been utilized for Xerography, a target of image pickup tubes and so on. Amorphous  $\text{As}_2\text{S}_3$  (a- $\text{As}_2\text{S}_3$ ) have attracted the attention as a material for optical memory devices, and for optical fibers for infrared light because of its good transparency in this wavelength region. Therefore, it is important to study the defect processes in chalcogenide glasses, which affect the efficiency of such devices.

Adequate understanding of the defect processes with photoexcitation in amorphous semiconductors depends on having information about the localized states in the forbidden gap, since it has been suggested that photogenerated carriers trapped at the localized states play an important role. Photoluminescence is an adequate technique for such an investigation. The technique is very sensitive to the localized states, compared to, for example, absorption spectroscopy.

a- $\text{As}_2\text{S}_3$  is hardly to be crystalized and its physical properties are not sensitive to impurities unlike the crystal semiconductors where the doping effects are observed. The sample dependence is not significant in a- $\text{As}_2\text{S}_3$ . Thus it is adequate to study the physics in amorphous semiconductors. Recently we have discovered a new kind of PL centers, which are created with band-gap irradiation. They are stable only at low temperatures and are associated with

the optically induced metastable states in a- $\text{As}_2\text{S}_3$ . This PL may be a useful probe for studying the optically induced phenomena in chalcogenide glasses. The purpose of this thesis is to study the detailed properties of the PL centers, to clarify the relation with other optically induced phenomena such as the PL fatigue and optically induced below-gap absorption in chalcogenide glasses, and to understand the defect processes in chalcogenide glasses, especially for the photoinduced defects stable only at low temperatures.

The following part of this thesis is as follows.

In the chapter 2, we describe briefly the optical phenomena in chalcogenide glasses which have been reported so far.

In the chapter 3, brief descriptions of the experimental apparatus and the measurements are given.

The experimental results are presented in the chapter 4, and are discussed in the chapter 5.

## Chapter 2

# A Brief Summary of the Optical Phenomena in Chalcogenide Glasses

### 2.1 ABSORPTION SPECTRA

In crystalline semiconductors, the absorption spectra have a sharp cut-off at the band-gap energy, around which the absorption coefficient,  $\alpha$ , for direct-gap-semiconductors can be written as:

$$\alpha \sim (h\nu - E_0)^{1/2}. \quad (2.1.1)$$

This is derived from a parabolic density of state with  $k$ -conservation rules.

However, in amorphous semiconductors, the absorption spectra do not have a sharp cut-off. Because of the lack of long range order, the density of states is non-zero at the band edge, and has tail states below in band-tail [Mott and Davis 1979]. The wavefunction in the band-tail is localized, the extent of which is a few atomic distances. Inside the band, however, the wavefunction is extended. Mott proposed that there is a mobility edge in the band, which separates the localized states and extended states. The absorption spectrum in amorphous semiconductors reflects this situation.

In chalcogenide glasses, there are three regions in the absorption spectrum, (A) the high absorption region, (B) the Urbach tail region, and (C) the weak absorption region as can be seen in fig.2.1.

In the high-absorption region A, where  $\alpha > 10^4 \text{cm}^{-1}$ , the absorption coefficient can be described [Tauc 1974] as

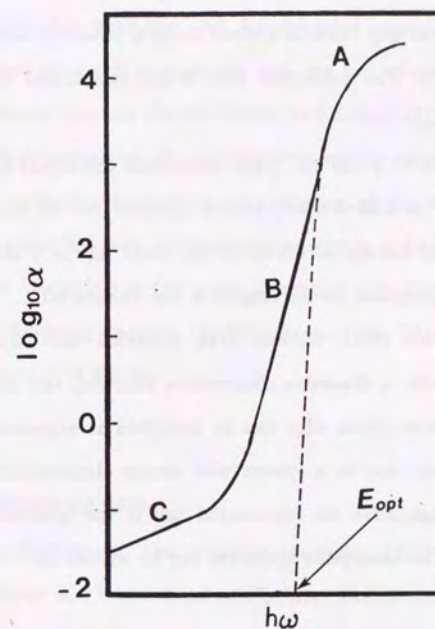


Figure 2.1

The three principal optical absorption bands in an amorphous semiconductor. A, B, and C are described in the text. The dashed line represents extrapolation of part A, using eq.(2.1.2). [Wood and Tauc 1972].

$$h\nu \alpha \sim (h\nu - E_{\text{opt}})^2, \quad (2.1.2)$$

where  $E_{\text{opt}}$  is the optical gap. This is derived from a parabolic density of states for electrons and holes. The  $k$ -selection rule is not maintained because of the lack of long range order.

In region B, where  $1 < \alpha < 10^4 \text{cm}^{-1}$ , the absorption coefficient is described as  $\alpha(\nu) \sim \exp(h\nu/E_c)$ .  $E_c$  is 0.05–0.08eV, almost identical for all the chalcogenide glasses. An exponential density of states of the band tail or a strong electron-lattice interaction are proposed as the origins of the Urbach tail.

Abe and Toyozawa [1981] showed that, provided that the site energy fluctuates randomly with a Gaussian distribution function, the density of state and the fundamental absorption edge can be described as exponential functions. Toyozawa [1964] showed that in a system with strong electron-phonon coupling, the absorption spectrum have an exponential tail if the quadratic interaction cannot be neglected. The absorption spectrum can be written as

$$\alpha = \alpha_0 \exp(\gamma(h\nu/kT)). \quad (2.1.3)$$

According to this equation, the slope of the Urbach tail decreases with temperature. However, at low temperature, the Urbach tail in chalcogenide glasses, except for a-Se, changes little. At high temperatures, eq.(2.1.3) is obeyed.

In the two models, the former is based on the spatial fluctuations of the energy levels and the latter on the thermal fluctuations. The Urbach tail in chalcogenide glasses is due to both spatial fluctuations of the energy levels and thermal fluctuations at low temperatures, and the effect of the thermal fluctuations is dominant at high temperatures.

Below the Urbach tail, there is another exponential tail, the weak absorption tail. The slope depends on the material, the preparation conditions, and the

thermal treatments [Wood and Tauc 1972], unlike the Urbach tail. Tauc proposed that the weak absorption tail is transitions between the defect (or impurity) states in the band-gap and the extended states in the band. On the other hand, Street *et al.* [1975] suggested that the tail arises from the absorption band due to phonon coupling [Street, Searle, and Austin 1975].

As was mentioned above, the band-gap energy in amorphous materials can not be defined definitely because of the presence of the tail states, unlike the situation in crystals. We take the band-gap energy in a-As<sub>2</sub>S<sub>3</sub> to be 2.2eV, which is the energy of beginning of the weak absorption tail. Furthermore, as we will mention in the following chapter, the properties of the PL in a-As<sub>2</sub>S<sub>3</sub> change at the excitation energy of 2.2eV.

## 2.2 PHOTOLUMINESCENCE

The main feature in the photoluminescence (PL) spectra of arsenic chalcogenide glasses is a broad band with a large Stokes shift. This suggests that the chalcogenide glasses have a strong electron-phonon coupling. The peak energy is centered at about half the band-gap energy. In fig.2.2, PL spectra measured at low temperatures (4–10K) in a-As<sub>2</sub>S<sub>3</sub>, a-As<sub>2</sub>Se<sub>3</sub>, and a-As<sub>2</sub>Se<sub>1.5</sub>Te<sub>1.5</sub> are shown, together with the absorption and the excitation spectra. The PL spectra are symmetrical and show no fine structures. They can be fitted with Gaussian curves. For various chalcogenide glasses, the peak position and the line width both increase as the band-gap energy increases [Street 1976]. The luminescence intensity is approximately the same for all the three glasses, whose maximum quantum efficiency is 10–20% at 4K. [Fischer *et al.* 1971, Street *et al.* 1973]

The observed PL spectrum of an as-evaporated As<sub>2</sub>S<sub>3</sub> film have a much broader line width of 1.0eV, compared to about 0.4eV for the bulk glass samples

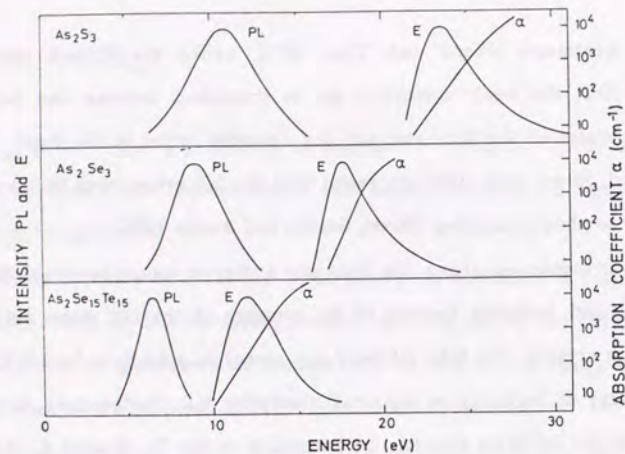


Figure 2.2

Low temperature PL, excitation spectra (E) and optical absorption ( $\alpha$ ) from amorphous  $\text{As}_2\text{S}_3$ ,  $\text{As}_2\text{Se}_3$ , and  $\text{As}_2\text{Se}_{1.5}\text{Te}_{1.5}$ . [Street 1976].

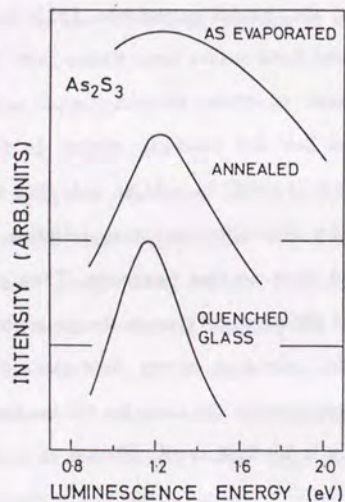


Figure 2.3

A comparison of the 10K PL spectra of evaporated and glassy  $\text{As}_2\text{S}_3$ . [Street *et al.* 1973].

(fig.2.3). After annealing the film at 473K, the line width becomes narrower and it is almost identical to that of bulk glass samples. The Raman scattering spectra of an as-evaporated film sample contain several relatively sharp lines, which are attributed to the vibrations of As-As or S-S bonds [Nemanich *et al.* 1978]. These lines decrease in intensity or disappear after annealing. This suggests that the as-evaporated film samples contain structural units such as  $\text{As}_4\text{S}_4$  molecules which are not present in the bulk samples, and they are polymerized in the glass networks by annealing.

Crystalline arsenic chalcogenides have similar PL spectra to those of glassy samples. The spectra of crystalline and amorphous  $\text{As}_2\text{Se}_3$  are compared in fig.2.4. The same broad symmetrical band is present with a similar half-width as that of the glass. The peak energy is higher by 0.2eV, and this is due to the larger band gap energy. It seems that the luminescence process in the crystalline phase is similar to that in the glassy phase. Thus, it is important to study the PL in crystalline samples.

The PL spectra in crystalline  $\text{As}_2\text{S}_3$  (c- $\text{As}_2\text{S}_3$ ) were reported by Kolomiets *et al.* [1970]. The peak energy is 1.26eV at 77K, slightly higher than that in amorphous samples. Mollot *et al.* [1974] also reported similar spectra with a peak energy slightly lower by 0.1eV. However, Street *et al.* [1974] and Bosch *et al.* [1980] reported a main PL band at 1.6eV.

Murayama and Bosch [1981] pointed out that these differences are not due to crystal quality but are rather due to different PL processes.  $\text{As}_2\text{S}_3$  crystals have not been grown in laboratories and, instead, naturally occurring minerals have to be used. They may contain impurities and defects. The absorption spectra in c- $\text{As}_2\text{S}_3$  were measured by Murayama and Bosch. They observed a shoulder at 2.5eV, which corresponds to a transition between a shallow defect (or impurity) level and the band edge. The excitation of this shoulder causes a PL spectrum with a peak energy of 1.53eV while band-to-band excitation causes PL

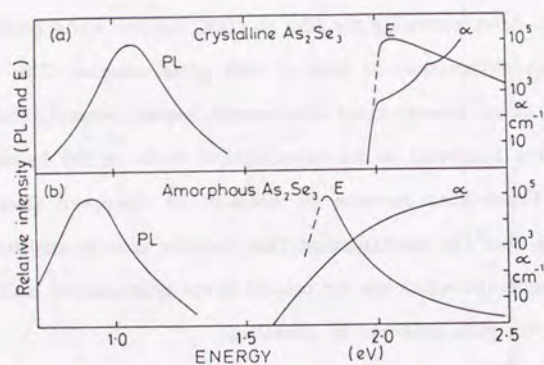


Figure 2.4

A comparison of the 10K PL spectra, excitation spectra (E) and optical absorption ( $\alpha$ ) from amorphous and crystalline  $\text{As}_2\text{Se}_3$  [Street *et al.* 1974d].

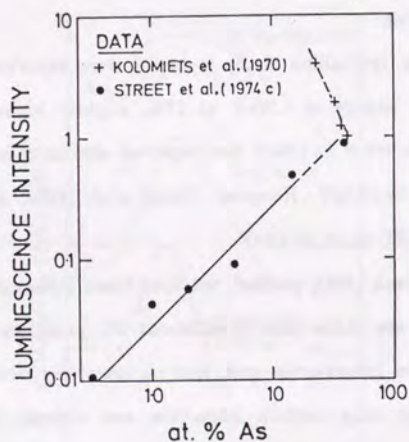


Figure 2.5

The variation of PL intensity with arsenic concentration in amorphous As-Se system. [Street *et al.* 1974b]

with a peak energy of 1.25eV. The excitation spectrum of the latter corresponds to the fundamental absorption. Therefore, it is an intrinsic PL in c- $\text{As}_2\text{S}_3$ .

In the amorphous As-Se system, Street *et al.* [1974b] find that the PL intensity is approximately proportional to the arsenic concentration, between 0.3 and 40 at.%As, as shown in fig.2.5. The peak position does not change through the amorphous As-Se system, although below 5 at.%As the intensity is so weak that the position cannot be accurately determined. The peak energy of a- $\text{As}_2\text{Se}_3$  is larger by about 0.1eV than that of a-Se, and a shift of about 0.1eV to the peak position of amorphous Se must occur at low As concentrations. It is suggested that arsenic sites play an important role in the PL process in As-Se systems, and this is also the case for other arsenic chalcogenides.

### 2.2.1 THE PHOTOLUMINESCENCE EXCITATION SPECTRA

The photoluminescence excitation (PLE) spectra are measured by monitoring the PL intensity whilst varying the excitation energy. They are normalized by the incident photon flux. The PLE spectra in chalcogenide glasses consist, generally, of a broad band, peaked at about the band-gap energy, as is shown in fig.2.2 [Street *et al.* 1973, Bishop 1973, Bishop and Mitchell 1973, Cernogora *et al.* 1973]. Evaporated  $\text{As}_2\text{S}_3$  films have a similar PLE spectrum. It is slightly changed by annealing at the glass transition temperature [Street *et al.* 1973].

The lineshape of a PLE spectrum is determined by the absorption coefficient and the PL quantum efficiency. The rapid decrease in the PLE of the chalcogenide glasses below the peak energy is not due to the decrease of the quantum efficiency. This is reflected in the absorption spectra. Street *et al.* [1974d] reported that the low energy side of the PLE spectra becomes constant when a correction,  $\exp(-\alpha d)$ , is made for the transmission, where  $\alpha$  is the absorption coefficient and  $d$  is the sample thickness. This suggests that the

quantum efficiency below the peak energy of the PLE is approximately constant.

Above the peak energy of the PLE spectra, the intensity is also reduced. The excitation energy is in the fundamental absorption region, and all the excitation light is absorbed. Therefore, this reduction is due to a reduction of the PL quantum efficiency. The reduction of the quantum efficiency with increase of excitation is often explained by surface recombination [de Vore 1956]. Bishop [1973] and Bishop and Mitchell [1973] explained the PLE spectra in chalcogenide glasses by this theory.

However, Street *et al.* [1974a] pointed out that it is not satisfactory and, instead, proposed that the decrease in the high energy side is due to the energy dependence of the internal quantum efficiency, since the diffusion length of the photo-excited carriers needs to be 2-3 microns in order to explain the decrease by surface recombination. This is unreasonably long in disordered systems such as the chalcogenide glasses. Furthermore, the line shape of the PLE spectra is little altered even if temperature is raised. This would imply that the diffusion length is independent of temperature. Thus surface recombination is not important, though it may be for  $\alpha$  above  $10^6 \text{cm}^{-1}$ , which corresponds to excitation energies larger than 3.0eV in a- $\text{As}_2\text{S}_3$ .

Saturation effects are not the reason for the decrease, since the PL intensity is proportional to the excitation intensity [Street *et al.* 1973, Mollot *et al.* 1974].

The energy dependence of the probability of capture into the radiative recombination centers can explain the effects [Street *et al.* 1974a]. Street *et al.* supposed that the carriers must be excited sufficiently close to the PL centers in order to radiatively recombine. If the carriers are excited far from the PL centers, they cannot recombine radiatively because of the low mobility in amorphous materials. Thus, the quantum efficiency,  $y$ , can be written as

$$y = \alpha_c(E) / \alpha(E), \quad (2.2.1)$$

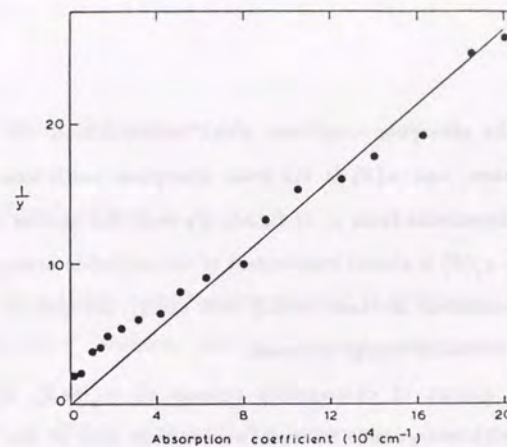


Figure 2.6

The inverse of the PL quantum efficiency are plotted as a function of optical absorption coefficient. [Street *et al.* 1974a].

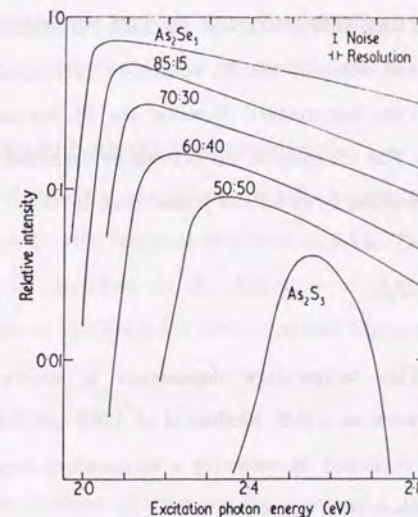


Figure 2.7

Excitation spectra of chalcogenide crystals of  $\text{As}_2(\text{S}, \text{Se})_3$  system at 10K. Numbers represent the relative atomic proportion of  $\text{As}_2\text{Se}_3$  and  $\text{As}_2\text{S}_3$  in the mixed crystals. [Street *et al.* 1974d]

where  $\alpha_c(E)$  is the absorption coefficient which corresponds to the absorption near the PL centers, and  $\alpha(E)$  is the total absorption coefficient.  $\alpha_c$  has a different energy dependence from  $\alpha$ . In fig.2.6,  $1/y$  is plotted against  $\alpha(E)$  for a-As<sub>2</sub>S<sub>3</sub>. As is seen,  $\alpha_c(E)$  is almost independent of the excitation energy. Since the total absorption coefficient increases rapidly with energy, the quantum efficiency is reduced as the excitation energy increases.

In the PLE spectra of chalcogenide crystals of As<sub>2</sub>(Se,S)<sub>2</sub> systems, the decrease in the high energy side is much weaker than that of the amorphous materials (fig.2.7). This is consistent with the above theory. The crystalline samples have a much longer diffusion length, and the photoexcited carriers in the crystals are able to reach the PL centers, even if they are excited far from the PL centers.

### 2.2.2 THE TEMPERATURE DEPENDENCE OF THE PL INTENSITY

The peak energy and width of the PL spectra in chalcogenide glasses are not strongly dependent on temperature. However the PL intensity is strongly temperature dependent. The intensity of PL ( $I$ ) can be described empirically as a function of the temperature,  $T$ , as follows [Street *et al.* 1974c]

$$I = I_0 \exp(-T/T_0), \quad (2.2.2)$$

where  $T_0 = 20-40$ K. This temperature dependence is widely observed in amorphous materials, such as a-Si:H [Collins *et al.* 1980] and a-SiO<sub>2</sub> [Gee and Kastner 1980]. This is explained by assuming a temperature dependence of the non-radiative recombination rate,  $p_{nr}$ , as:

$$p_{nr} = W_0 \exp(T/T_0). \quad (2.2.3)$$

The PL intensity,  $I$ , is written as:

$$I(T) = G \cdot p_r / (p_r + p_{nr}), \quad (2.2.4)$$

where  $p_r$  is the radiative recombination rate and  $G$  is the generation rate. Thus, if the temperature increases, and  $p_{nr}$  becomes much larger than  $p_r$ , then  $I \sim \exp(-T/T_0)$ .

Street *et al.* [1974c] explained this exponential dependence of the non-radiative recombination rate by phonon-assisted tunneling through weak potential fluctuations. That is, electron-hole pairs are ionized by phonon-assisted tunneling as the temperature rises. This is not the only explanation possible. Gee and Kastner [1980] explained the temperature dependence by assuming exponential distribution of the activation energies to non-radiative recombination channels. Street [1984] also explains the same dependence in a-Si:H based on the activated release of carriers from the exponential band tail to the mobility edge.

### 2.2.3 TIME RESOLVED PHOTOLUMINESCENCE

The decay of the PL intensity after a pulsed excitation in a-As<sub>2</sub>S<sub>3</sub> consists of three components with different life-times at 4.2K. The time-decay of each component can be described as the derivative of the stretched exponential functions [Murayama and Ninomiya 1982, Ngai and Murayama 1982]

$$f(t) = t^{\beta-1} \exp[-(t/\tau)^\beta]. \quad (2.2.5)$$

$\tau$  is the effective life-time.  $f(t)$  becomes the exponential decay function when  $\beta$  is equal to 1. The life-times of each component are  $2 \times 10^{-8}$ s,  $2 \times 10^{-6}$ s, and  $2 \times 10^{-4}$ s, and are called the fast decay component, the intermediate decay

component, and the slow decay component, respectively. The peak energies of the time resolved PL spectra decrease with time [Higashi and Kastner 1981].

The slow decay component is attributed to the recombination of triplet excitons [Depinna and Cavenett 1982a, Robins and Kastner 1984, 1987, Tada *et al.* 1984].

#### 2.2.4 ODMR MEASUREMENTS

Measurements of optically detected magnetic resonance (ODMR) reveals detailed information on the PL centers.

ODMR studies in  $a\text{-As}_2\text{S}_3$  were made by Suzuki *et al.* [1979], Suzuki [1982], Tada *et al.* [1984], and Depinna and Cavenett [1982a]. They observed two kinds of signals, which were attributed to the resonance of triplet excitons (the triplet resonance) and that of distant electron pairs (the pair resonance). The triplet resonance consists of broad double peaks with  $g=6.0$  and  $2.3$  (fig.2.8). The pair resonance is a relatively narrow peaks with  $g=2.0$ . Depinna and Cavenett showed that ODMR spectra in  $a\text{-As}_2\text{Se}_3$  [1982b] and  $a\text{-P}$  [1982c] are similar to that of  $a\text{-As}_2\text{S}_3$ .

Tada *et al.* showed that the width of the pair resonance is due to an unresolved hyperfine structure. Since a S-nucleus has no spin, the hyperfine structure is due to an As-nucleus ( $I=3/2$ ). Thus the pair resonance is associated with As atoms. Suzuki showed that the relative intensity of the pair resonance decreases as the sulfur content increases in  $a\text{-As}_x\text{S}_{1-x}$  (fig.2.9). This is consistent with the above observation.

For crystalline  $\text{As}_2\text{S}_3$  [Suzuki 1982] and  $\text{As}_2\text{Se}_3$  [Depinna and Cavenett 1982b, 1983, Robins and Kastner 1987], the ODMR spectra is similar to that of the amorphous phases, when excited with energy slightly lower than the band-gap energy (fig.2.10, 2.11). In this case, both pair resonance and triplet resonance are observed. However, Ristein *et al.* [1989] reported that when excited with above-

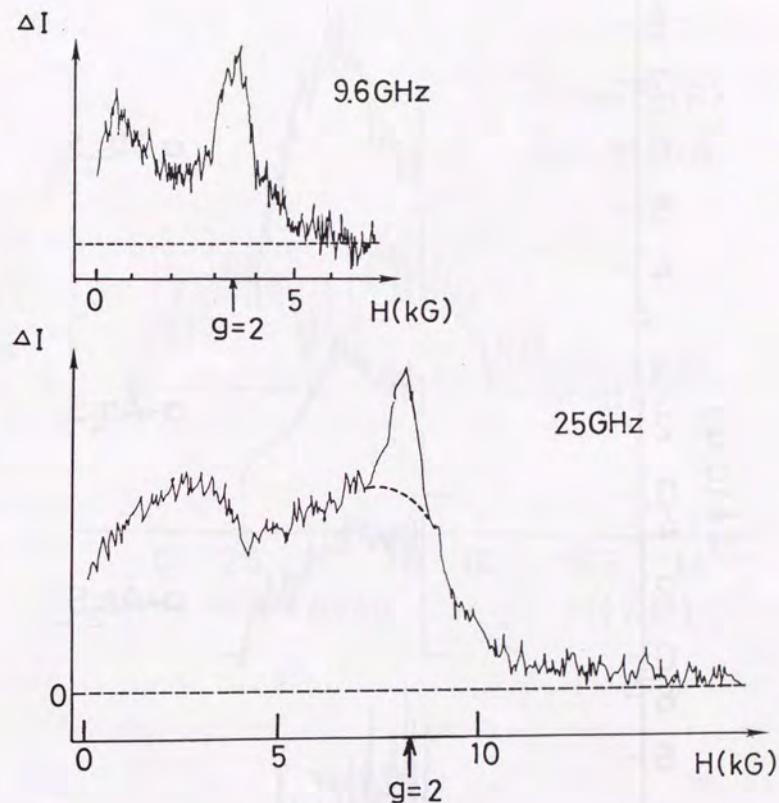


Figure 2.8

The ODMR spectra for the microwave frequency of 9.6GHz and 25GHz. The excitation energy was 2.41eV and the total emission was monitored. [Tada *et al.* 1984].

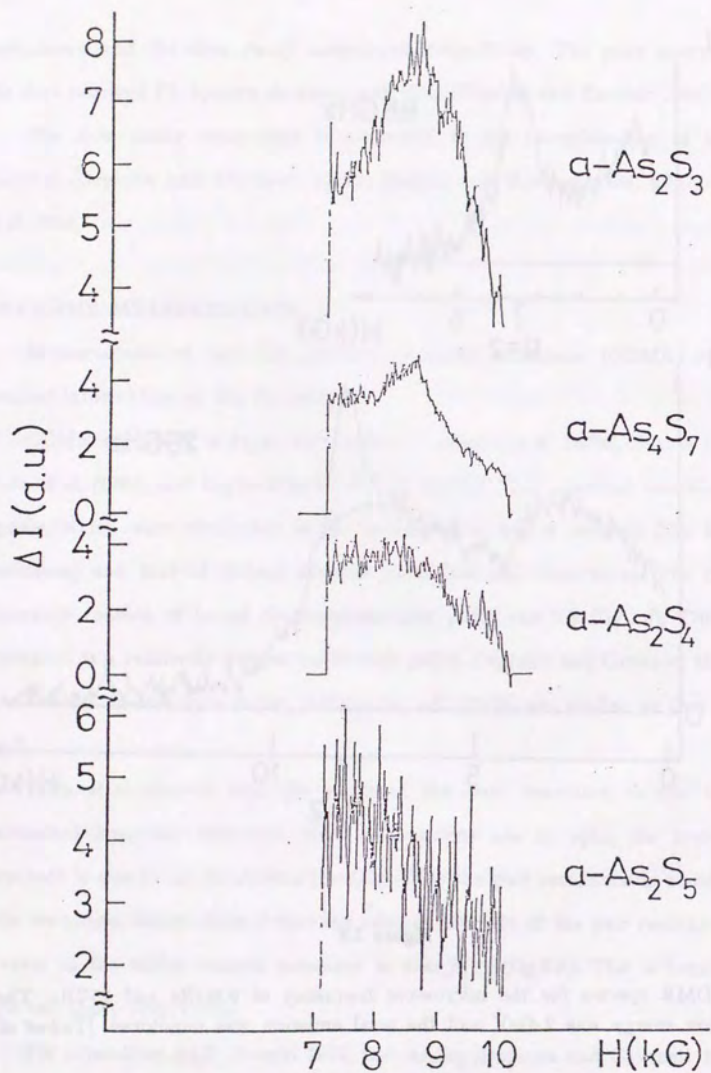


Figure 2.9

The pair resonance in  $\alpha\text{-As}_2\text{S}_{1-x}$  is represented for various sulfur concentration. [Suzuki 1982].

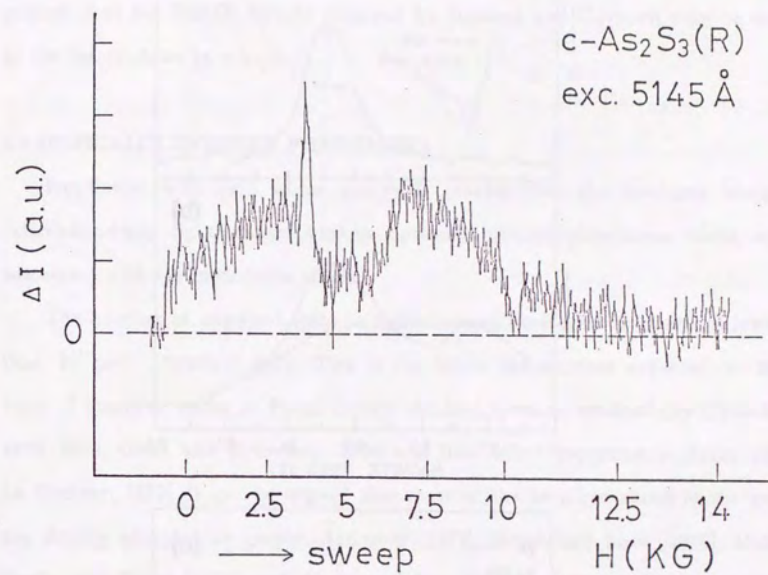


Figure 2.10

The ODMR spectrum of  $c\text{-As}_2\text{S}_3$ . The excitation energy is 2.41eV. a-axis is parallel to the external magnetic field. [Suzuki 1982].

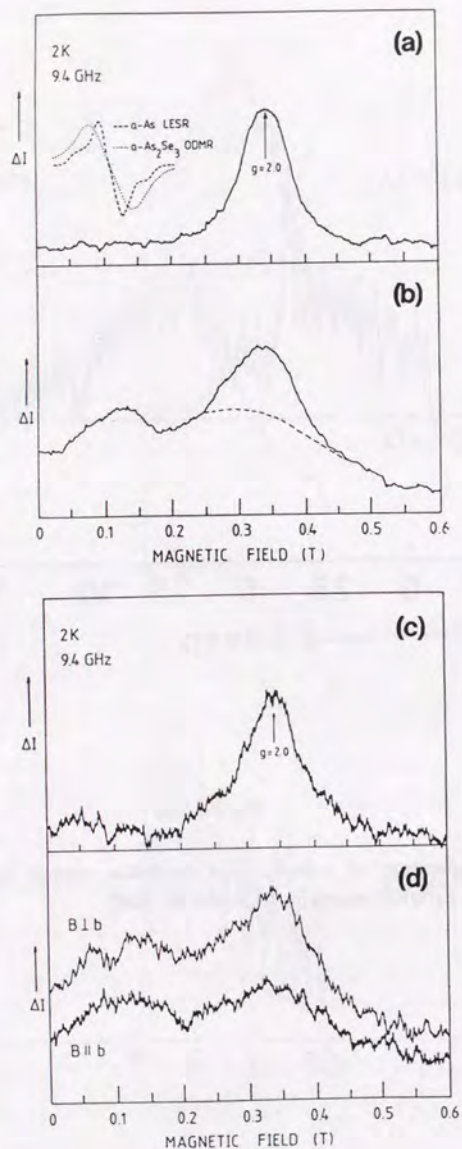


Figure 2.11

The ODMR spectra of (a), (b) a-As<sub>2</sub>Se<sub>3</sub> and (c), (d) c-As<sub>2</sub>Se<sub>3</sub> are represented. The excitation energies are (a) 1.83eV, (b) 1.65eV, (c) 1.92eV, and (d) 1.65eV. [Depinna and Cavenett 1982b].

gap light, only the triplet resonance is able to be observed in c-As<sub>2</sub>Se<sub>3</sub>. They pointed that the ODMR signals observed by Depinna and Cavenett may be due to the defect states in c-As<sub>2</sub>Se<sub>3</sub>.

### 2.3 OPTICALLY INDUCED PHENOMENA

Irradiation with light whose energy is greater than the band-gap energy (above-band-gap light) causes various optically induced phenomena which are associated with the metastable states.

The number of unpaired spins in well-annealed chalcogenide glasses is lower than  $10^{14}\text{cm}^{-1}$  [Agarwal 1973]. This is far below the number expected on the basis of localized states at Fermi energy obtained from ac conductivity [Fritzsche 1973, 1974, Owen and Robertson, 1970] and field effect experiments [Spear and Le Comber, 1972]. It can be argued that most of the localized states in the gap are doubly occupied or empty. Anderson [1975], Street and Mott [1975], Mott, Davis, and Street [1975], and Kastner, Adler, Fritzsche [1976], and Emin [1980] proposed models which explain the double or empty occupancy on the basis of the strong electron-phonon interaction in the chalcogenide glasses.

Bishop *et al.* [1975, 1977a] first observed the optically induced localized paramagnetic states in the band gap of chalcogenide glasses. Irradiation of chalcogenide glasses, such as Se, As<sub>2</sub>Se<sub>3</sub>, and As<sub>2</sub>S<sub>3</sub>, with above-band-gap light at low temperature produces ESR centers which are not present in the equilibrium cold-dark state. They also found that the irradiation produces below-gap absorption at low temperatures. The optically induced ESR (or light induced ESR: LESR) and the below-gap absorption are stable at low temperature. Irradiation with above-band-gap light reduces the intensity of PL intensity in chalcogenide glasses. This is called photoluminescence fatigue [Cernogora *et al.* 1973, Street *et al.* 1973, Mollot *et al.* 1974]. The PL fatigue is also stable at low temperatures.

In the following section, we will examine the optically induced phenomena in more detail.

### 2.3.1 OPTICALLY INDUCED ESR AND BELOW-GAP ABSORPTION BAND

As was mentioned above, the above-band-gap irradiation causes the LESR centers and the optically induced below-gap absorption band (fig.2.12, 2.13). The absorption band appears in the energy range from  $E_g/2$  to  $E_g$ , where  $E_g$  is the band-gap energy. The LESR centers and the absorption band are annealed as temperature rises [Bishop *et al.* 1977b]. In a-As<sub>2</sub>Se<sub>3</sub>, they are annealed out at 180K. The same effects are observed in other chalcogenide glasses. They are also bleached by infrared irradiation whose energy is within the optically induced absorption band [Bishop *et al.* 1977a].

The LESR signal in an arsenic chalcogenide glass is a superposition of a narrow line related with holes localized on the chalcogen atoms and a broad line related with electrons localized on arsenic atoms [Bishop *et al.* 1977a]. In a-As<sub>2</sub>S<sub>3</sub>, the low-energy-irradiation ( $E_{exc} < 1.8\text{eV}$ ) produces mainly chalcogen hole centers, and the As-related centers increasingly contribute to ESR line shape as the excitation energy increases [Freitas *et al.* 1987, Strom *et al.* 1987].

It has been found that the excitation intensity affects the properties of the photo-induced centers [Bernoit *et al.* 1977, Biegelsen and Street 1980, Frietas *et al.* 1985]. At low irradiation intensity, the spin density saturates at  $\leq 10^{17}\text{cm}^{-3}$ . It has been suggested that this saturation is a result of the trapping of photoexcited carriers at defects, and their frozen-in concentration limits the saturation of the induced spin density [Bishop *et al.* 1975, 1977a]. At high excitation intensity ( $>100\text{mW/cm}^2$ ), Mollot *et al.* have found that the spin density does not saturate and exceeds  $10^{20}\text{cm}^{-3}$  after prolonged above-band-gap irradiation [Bernoit *et al.* 1977]. Gaczi [1982] studied the optically induced ESR in As-S glasses of various compositions and found that the ESR signal of

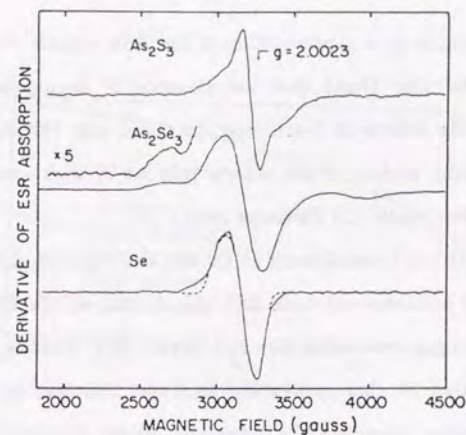


Figure 2.12

Optically induced ESR signals in chalcogenide glasses at 4.2K. Dashed line superimposed in Se curve is a computer simulation. [Bishop *et al.* 1977a].

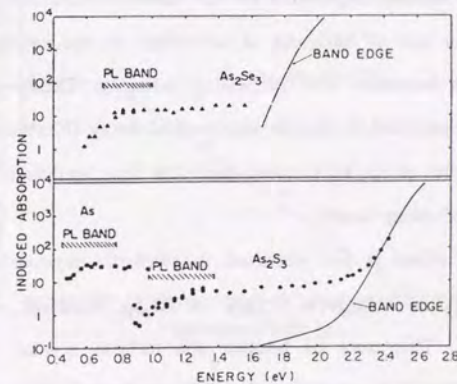


Figure 2.13

Optically induced below gap absorption for a-As<sub>2</sub>Se<sub>3</sub> and a-As<sub>2</sub>S<sub>3</sub> indicated by solid circles. Preillumination band-edge absorption curves are also given. [Bishop *et al.* 1977a].

stoichiometric sample is a superposition of the ESR signals from arsenic and sulfur defects. He also found that the presence of homopolar S-S bonds is associated with the defects in S-rich sample. Gaczi and Fritzsche discussed the possible microscopic models of the defects induced by high excitation intensity for As-rich samples [Gaczi and Fritzsche 1981].

Addition of Group I metals such as Cu into chalcogenide glasses reduces the LESR signal but enhances the dark ESR signal, that is, the ESR signal which exists before band-gap irradiation [Liu and Taylor 1987, Hautala *et al.* 1989]. The average coordination of chalcogen atoms increases from two to eventually four due to the addition. Therefore the 'flexible' glasses become 'rigid' and the electron-phonon interaction decreases, leading to suppressing the optically induced phenomena.

### 2.3.2. PHOTOLUMINESCENCE FATIGUE

Since the first observation of PL fatigue by Cernogola *et al.* [1973], the PL fatigue has been of central importance for the electronic structure of amorphous semiconductors. The rate of fatiguing is dependent on the irradiation intensity and wavelength. It increases with increasing intensity. Time-evolution of the fatigue cannot be described by simple exponential decay [Kastner and Hudgens 1978] (fig.2.14). Mollot *et al.* [1974] noted that this time evolution arises from a broad distribution of decay times.

The fatiguing effect is not observed in synthetic crystals of  $As_2S_3-xSe_x$  [Street *et al.* 1974d]. In a natural crystal of  $As_2S_3$ , orpiment, it is observed [Mollot *et al.* 1974]. This may be because the natural crystal contains more defects and impurities. It is noted that the PLE spectrum in the natural crystals of  $As_2S_3$ , which show the fatiguing effect, has a fast decrease in the high energy side [Street *et al.* 1974d].

The fatigue can be reversed by either heating or by infrared irradiation.

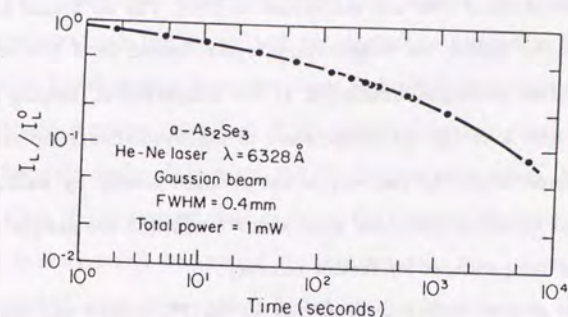


Figure 2.14

Time dependence of photoluminescence fatigue. [Kastner and Hudgens 1978]

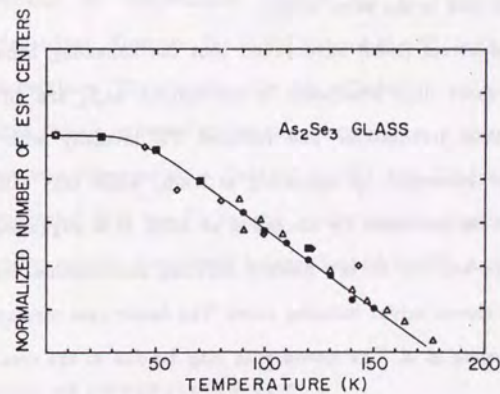


Figure 2.15

Temperature dependence of LESR centers (circles and squares) and optically induced absorption (triangles), and fraction of PL fatigue (diamonds). [Bishop *et al.* 1977b].

From the data of 'isochronal annealing', Mollot *et al.* [1974] showed that the recovery begins at about 50K and is complete at 250K. The isochronal annealing was performed by raising the temperature to the desired level (the annealing temperature) after prolonged irradiation at low temperatures, keeping it for 5 minutes, and then lowering the temperature to the irradiation temperature. At any chosen temperature, full recovery is not obtained merely by waiting for a long time. The annealing saturates after about 2 min and the sample must be taken to higher temperatures for further recovery.

There are similar annealing properties in the PL fatigue and the optical induction of ESR and the below-gap absorption. Bishop *et al.* [1977b] observed an identical thermal annealing behavior in these phenomena as shown in fig.2.15. They pointed out that the thermal release or reactivation of the optically induced paramagnetic centers, the optically induced absorption centers, and the fatigued PL centers is controlled by the same process. It seems that these phenomena are all due to the same origin.

Biegelsen and Street [1980] have found that the annealing behavior of the PL fatigue with short time irradiation in amorphous  $As_2S_3$  are different from that with long time irradiation. The fatigued PL intensity with short time irradiation can be recovered by annealing at 150K, while that with long time irradiation cannot be recovered by annealing at 150K. It is suggested that these different behaviors are due to two distinct inducing mechanisms, corresponding to a faster and a slower initial inducing rates. The faster rate corresponds to the observation by Bishop *et al.* The slower rate may be due to the creation of new defects.

The mechanism of PL fatigue is controversial. Following the discussion given by Mollot *et al.* [1974], Cernogola *et al.* [1974], Bishop *et al.* [1975, 1976], and Street [1976, 1978], the fatigue implies that after excitation the recombination centers can take up a new metastable state which is inefficient for luminescence.

PL centers are assumed to be charged [Mott *et al.* 1975]. If a photon is absorbed near the PL centers (say a negative center), the hole is captured deep in the band gap, neutralizing the center, and the electron is trapped in the band tail states nearby. Luminescence may take place, Stokes-shifted because of the strong electron-phonon coupling. However, if the electron escapes from the captured hole by thermally induced hopping, the PL fatigue takes place. Luminescence can take place if the trapped hole captures the electron. However, the capture rate may be very small because of the low diffusion rate, particularly if the center is neutral, since then capture is not assisted by Coulomb attraction. To reverse the fatigue, the trapped hole must be released from the recombination center.

Kastner and Hudgens [1978] proposed that the fatiguing process is not closely coupled to the luminescence process. If the PL fatigue is caused by the escape of an electron from the recombination center, the fatigue rate must be strongly dependent on temperature, because the PL intensity is strongly temperature dependent. However, the initial rate of the PL fatigue depends only weakly on temperature. The hopping rate are affected by an electric field and, thus, the fatigue rate is expected to become larger under a strong electric field. No such effect was observed in a field of  $2 \times 10^5$  V/cm [Hudgens and Kastner 1977]. They suggested that the PL fatigue results by the creation of non-radiative recombination centers, completely independent of the PL centers.

#### 2.4 STRUCTURE OF CRYSTALLINE $As_2S_3$

The structures of amorphous materials are not completely different from those of the crystalline phases. The long range order is not present in amorphous phases, while the short range order exists and is similar to the crystalline phases. Therefore, in order to realize the properties of a- $As_2S_3$ , the

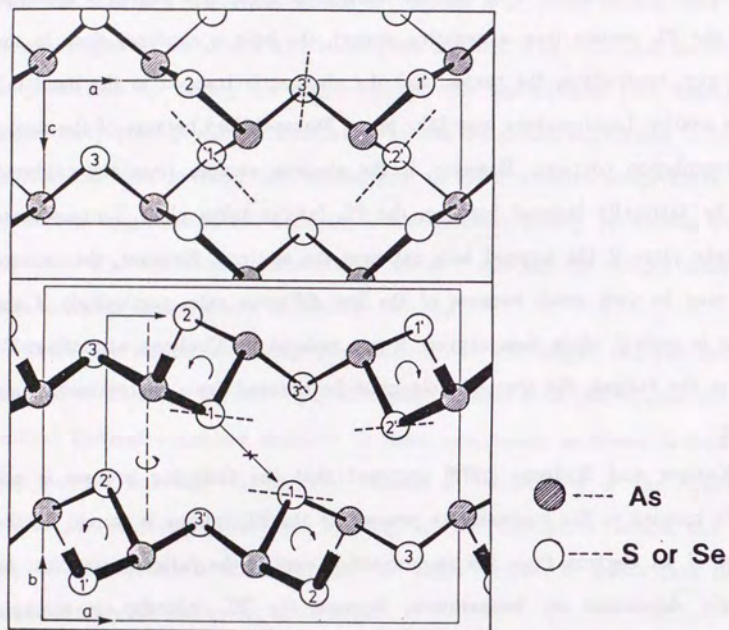


Figure 2.16

Structure of  $a\text{-As}_2\text{S}_3$  ( $a\text{-As}_2\text{Se}_3$ ) are represented. [Ristein and Weiser 1989].

crystal structure of  $\text{As}_2\text{S}_3$  are discussed briefly in this section. The structures of  $\text{As}_2\text{Se}_3$  is almost the same.

The lattice is built up by chains of alternating S and As atoms spiraling along the  $c$ -axis. Left and right handed chains are connected by S bridging atoms which leads to a covalently bound layer. Interlayer bonds are very weak with van der Waals interaction.

This layer structure gives flexibility to  $\text{As}_2\text{S}_3$ , and may be a key realizing the defect creation processes in the chalcogenide glasses.

# Chapter 3

## Experimental

### 3.1 SAMPLE PREPARATION

Samples of  $\alpha\text{-As}_x\text{S}_{1-x}$  were produced from elemental arsenic and sulfur of 99.9999% purity. Quartz ampoules were immersed in aqua regia for several hours and rinsed with pure water. The ampoules were evacuated and baked for about 12 hours. Then the elements were sealed in the evacuated ampoules, heated to 610°C, held in a rocking furnace for about 24 hours, and air quenched to room temperature. The values of  $x$  were limited upto 0.43 because the samples with  $x > 0.43$  contain polycrystalline material. The samples were cut into an appropriate size and the both sides were polished with diamond paste. Mirror surfaces were obtained.

### 3.2 PHOTOLUMINESCENCE MEASUREMENT

The block diagram of the experimental system for the PL measurements is presented in fig.3.1.

For below-gap excitation, we mainly used an AlGaAs high power laser diode (SONY SLD302V: 783nm, 1.58eV). A dye-laser pumped with an excimer laser (Lambda Physik EMG50) was also utilized for measuring the excitation energy dependence of the PL spectra and for the time resolved measurements. Samples were irradiated with either 514.5nm (2.41eV) or 528.7nm (2.35eV) line from an Ar<sup>+</sup>-laser (NEC GLG3200) to generate PL2 centers. The irradiation intensity and time were  $10^2 \sim 10^3 \text{mW/cm}^2$  and about an hour, respectively, which correspond to strong and long-time irradiation as was mentioned in the preceding chapter.

For steady-state PL measurements, optical excitation was provided by the laser diode or the Ar<sup>+</sup>laser. Excitation light was chopped at 20Hz with a duty

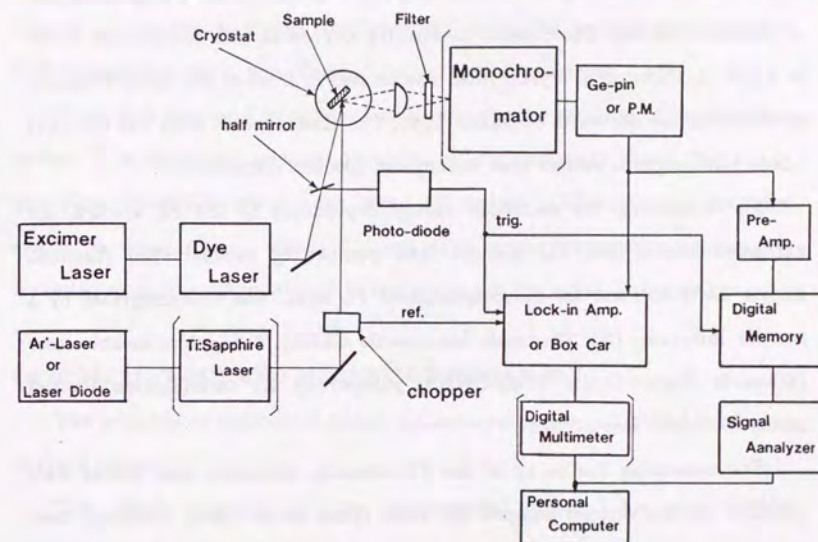


Figure 3.1

Block diagram of the experimental system for the PL measurements. The monochromator was not used for measuring the PL decay.

cycle of 0.5. This frequency is slow enough compared with the life time of the PL. Modulated PL was analyzed by a 22cm-monochromator (SPEX 1680B), detected with a cooled Ge-detector (North Coast EO-817L) and a lock-in amplifier (Stanford SR530). The detector is sensitive to photons with energy from 0.7eV to 1.5eV. A GaAs or Si crystal filter was located in front of the monochromator to eliminate the scattered excitation light. The GaAs and Si filter cut out light whose wavelength is shorter than 900nm and 1000nm, respectively.

For measuring the excitation energy dependence of the PL spectra, the excitation source used was the dye laser pumped by excimer laser (Lambda Physik EMG 50), and the monochromatized PL signal was time-integrated by a box-car integrator (NF Electronic Instruments BX531). Ti:Sapphire tunable laser (Schwartz Electro-Optics Titan-CWBB) pumped by Ar<sup>+</sup>-laser(Spectra Physics model 2016) was also utilized.

For measuring the decay of the PL intensity, excitation laser pulses were provided by the excimer-pumped dye laser (pulse width~20ns). Scattered laser light was eliminated by the GaAs or the Si crystal filter. The PL was detected with Ge-PIN diode detector (North Coast EO-817P: rise time ~200ns) or a photomultiplier tube of S1 type and the signals were processed with a transient waveform recorder (Digital memory DM901, Iwatsu) whose output was transferred to a signal averager (Signal analyzer SM2100A, Iwatsu). In this experiment, a monochromator was not used, and the light emission in the energy range where the photo-detectors have sensitivity was all detected.

Samples were immersed in liquid He in an optical Dewar for measurements at 4.2K.

An Oxford CF1204d continuous flow cryostat with temperature controller was utilized for 'isochronal annealing'. Samples were irradiated with band-gap-light at low temperature (irradiation temperature, usually 4.2K) to generate optically-induced metastable states. Isochronal annealing was performed by

raising temperature to the desired level (annealing temperature) and keeping it for 10 minutes and then lowering the temperature to the irradiation temperature. This procedure was then repeated at higher annealing temperatures. Annealing time of 10 minutes is enough for isochronal annealing because no significant further annealing effect was observed for an annealing time of 1 hour.

While it is not usual to correct line spectra for the response of the detection system, it is absolutely essential to correct PL spectra such those observed in amorphous materials, which have broad PL spectra. Calibrating the detection system is done with a standard lamp. The photoluminescence spectra are corrected so as to be proportional to the number of the emitted photons.

### 3.3 OPTICALLY INDUCED MAGNETIC RESONANCE

The principle of optically detected magnetic resonance (ODMR) is explained in the Appendix.

The block diagram of the experimental system for the ODMR measurements is presented in fig.3.2.

ODMR measurements were made at 1.6K with K-band (25GHz) microwave. Microwave source for K-band was klystron (OKI 24V11). The microwave cavity has a small hole through which excitation light from the Ar<sup>+</sup>-laser (Spectra Physics model 165-09) reach a sample and slits through which emitted light from the sample is taken out. The emitted light is collected by a lens and is led to the Ge-pin detector (EO-817P) through a quartz optical guide. In order to cut the excitation light, a color glass filter (IR80, HOYA) was used. The microwave is turned on and off by modulating the repeller voltage of the klystron and the excitation light is kept on continuously. The ESR signal is obtained as the synchronous change in the luminescence intensity using a lock-in detection method.

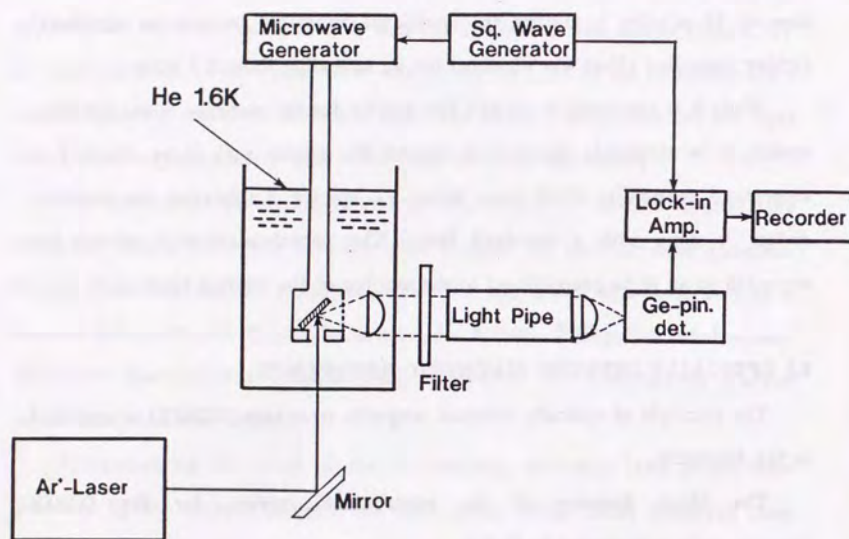


Figure 3.2

Block diagram of the experimental system for the ODMR measurement.

## Chapter 4

### Results

#### 4.1 PL1 and PL2

Photoluminescence (PL) spectra excited with 2.41eV light at 4.2K are shown in fig. 4.1 (a). The peak energy and the full width at half maximum (FWHM) are 1.1eV and 0.52eV, respectively. This is the photoluminescence which has been reported by many authors, and we call it PL1. The intensity of the PL1 is reduced after irradiation with 2.41eV light, which is so-called fatigue.

The PL spectrum excited with 1.58eV light before and after irradiation with 514.5nm (2.41eV) light at 4.2K is shown in fig.4.1(b). Before irradiation the PL intensity is very weak. The PL intensity, however, is enhanced after irradiation for an hour. The peak energy is slightly shifted to a lower energy after band-gap irradiation. As is seen, the PL excited with 1.58eV light is quite different from PL1.

Decay of photoluminescence with below-gap pulsed excitation at 4.2K is shown in fig.4.2. The excitation energy is 1.68eV. The decay curves are quite different for before and after the band-gap irradiation. This shows that a new kind of PL centers are created by the band-gap irradiation, and we call this new photoluminescence PL2. The dashed line in fig.4.1(b) is the spectrum in which the unirradiated base line is subtracted and represents the component enhanced by the irradiation, which corresponds to PL2. The FWHM of PL2 is about 0.38eV. The peak energy of PL2 is 0.85eV, which is about 0.25eV lower than the peak energy of the PL1 excited with 2.41eV.

The reason why the peak energy of PL1 shifts to lower energy after band-gap irradiation is that PL2 is also excited with 2.41eV light, and that a small fraction of the low energy part of the PL excited with 2.41eV light is PL2.

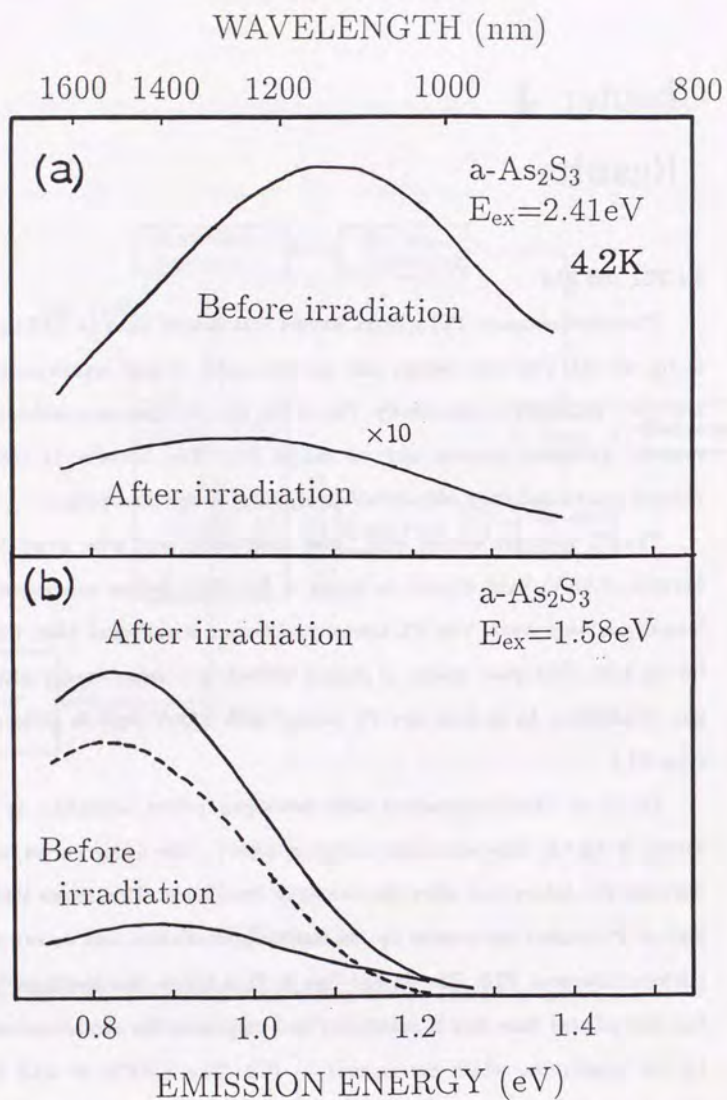


Figure 4.1

(a) PL spectra with excitation energy of 2.41eV before and after band-gap irradiation, which are denoted as PL1. The irradiation energy is 2.42eV. They are measured at 4.2K. (b) PL spectra with excitation energy of 1.58eV before and after band-gap irradiation. The irradiation energy is 2.41eV. The dashed line is the spectrum in which the unirradiated base line is subtracted and corresponds to PL2.

#### 4.2 EXCITATION ENERGY DEPENDENCE OF PL

As shown in the preceding section, the properties of PL in a-As<sub>2</sub>S<sub>3</sub> change with the varying of the excitation energy. In this section we will examine it in detail. The dependence of the peak energy of the emission spectrum in a-As<sub>2</sub>S<sub>3</sub> on the excitation energy is shown in fig.4.3. The sample had been irradiated for about an hour at 4.2K with 2.41eV light before this measurement. The peak energy  $E_p$  shifts at the excitation energy of about 2.2eV. Below 2.2eV,  $E_p$  is about 0.85eV while above 2.2eV  $E_p$  is 1.02eV. The effect of band-gap irradiation is also quite different depending on the excitation energy. In fig.4.4, the excitation spectra before and after the band-gap irradiation at 4.2K are shown. The total intensity of PL with excitation energy above 2.1eV is reduced by the irradiation with 2.41eV light (fatigue), while for the excitation energy below 2.1eV it is enhanced. To see it more clearly, the ratio of PL intensity after the band-gap irradiation to that before the irradiation is plotted as a function of the excitation energy, in fig.4.5.

There seems to be a separation energy  $E_s$  which divides the excitation energy ( $E_{ex}$ ) into two regions, one corresponding to the excitation of PL1 ( $E_{ex} > E_s$ ), and the other to PL2 ( $E_{ex} < E_s$ ).  $E_s$  is around 2.2eV. The optically induced absorption band observed by Bishop *et al.* are shown in fig.4.6. It seems that the PL2 centers are the same as the centers of the optically induced absorption band because the absorption band in a-As<sub>2</sub>S<sub>3</sub> appears below about 2.2eV [Bishop *et al.* 1977]. But this is not the case as will be shown in the next section.

#### 4.3 ANNEALING PROPERTIES OF PL CENTERS

The PL2 center are annealed out at room temperature. In order to examine the detailed behavior of annealing of the PL2 centers, isochronal annealing measurements were carried out. They show that the annealing properties of the

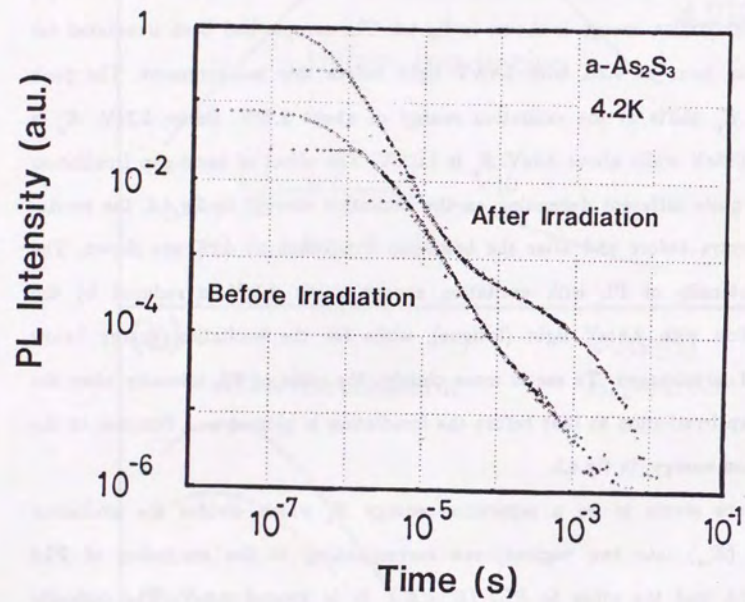


Figure 4.2

Decay curves of PL intensity with excitation energy of 1.68eV before and after band-gap irradiation are shown in log-log plot. The emitted photons of energy range from 0.7 to 1.2eV are detected. The line shapes of the decay curves are different for before and after the irradiation.

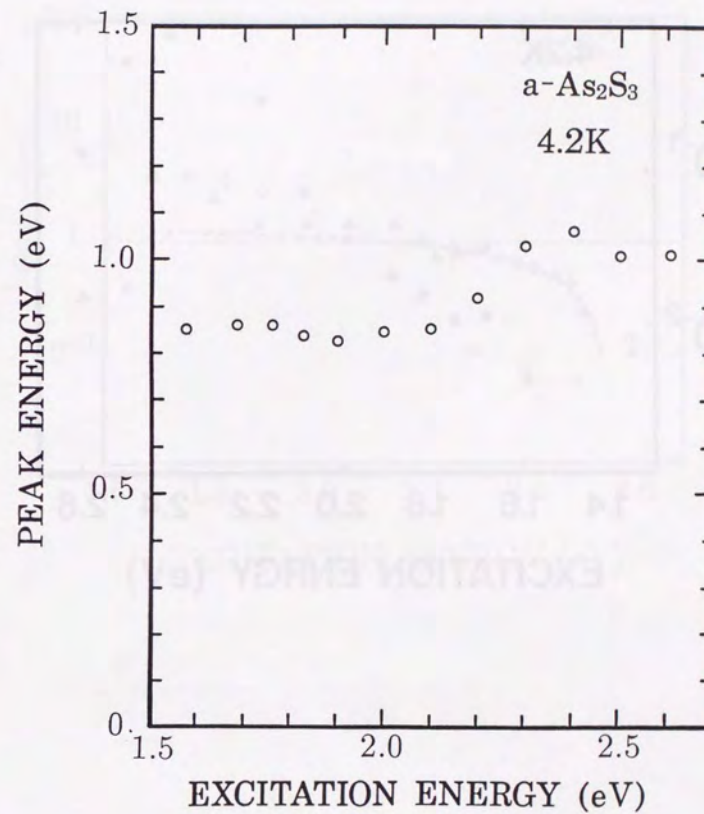


Figure 4.3

The peak energies of PL are plotted as a function of excitation energy. They are measured after band-gap irradiation at 4.2K.

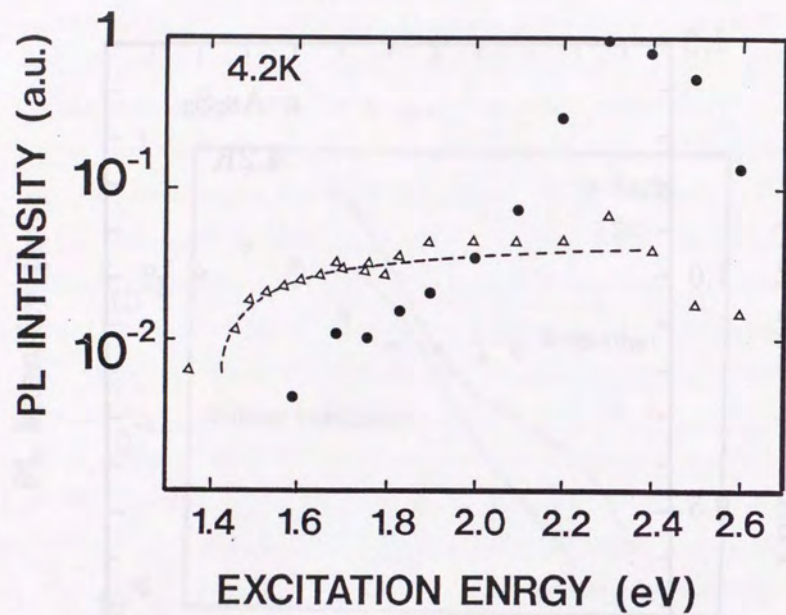


Figure 4.4

Photoluminescence excitation spectra before (●) and after (▲) band-gap irradiation are shown. The total PL intensity was monitored. The dashed line is a calculated curve described in the section 5.2.1. The intensity is normalized by the incident photon flux.

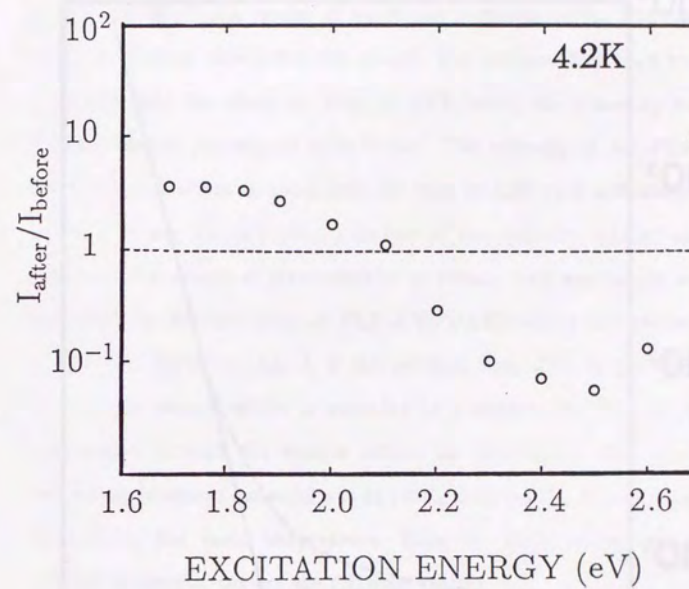


Figure 4.5

The ratio of PL intensity after band-gap irradiation to that before the irradiation is plotted as a function of excitation energy. The detected emission energy is 0.82eV.

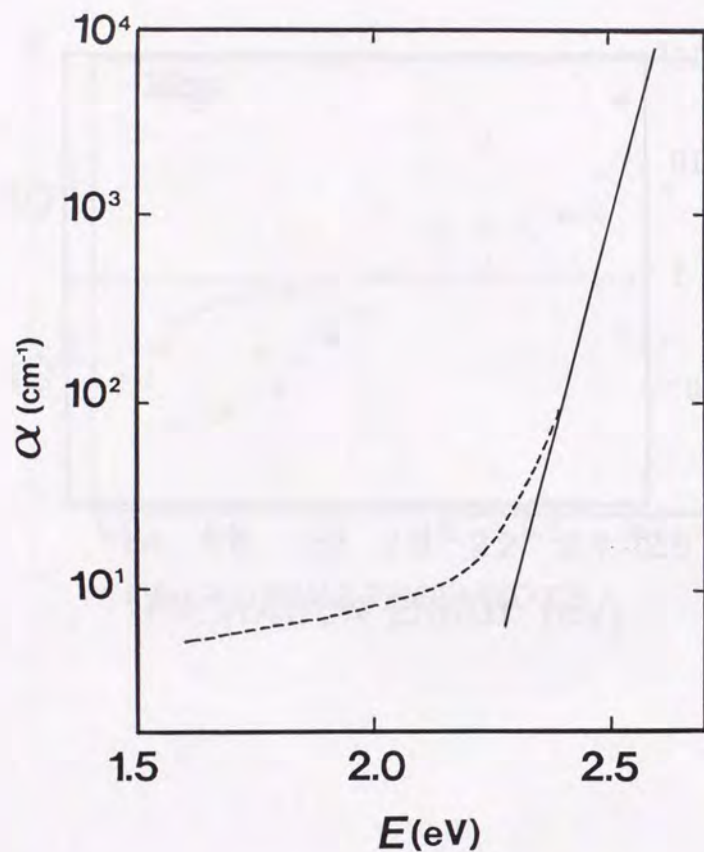


Figure 4.6

The absorption spectrum in a-As<sub>2</sub>S<sub>3</sub> is shown. The dashed line is the optically induced below-gap absorption. [Bishop *et al.* 1977a].

PL2 centers are quite different from that of the optically induced absorption centers. In fig.4.7, the results of isochronal annealing of the PL2 centers and the optically induced absorption are shown. The samples had been irradiated with band-gap light for about an hour at 4.2K before the annealing measurements. The irradiation intensity is 300mW/cm<sup>2</sup>. The intensity of the PL2 annealed at several temperatures is normalized by that at 4.2K (not annealed) and denoted by (○). To see the annealing behavior of the optically induced absorption, we measured the change of transmissivity at 783nm. This wavelength is the same as that used for the excitation of PL2.  $\Delta T(T)/\Delta T(4.2K)$  is also plotted ( $\Delta$ ), where  $\Delta T(T) = (J_i - J(T)) / (J_i - J_0)$ ,  $J_i$  is the incident flux,  $J(T)$  is the flux transmitted through the sample which is annealed at a temperature  $T$ , and  $J_0$  is the flux transmitted through the sample before the irradiation. The optically induced absorption is almost annealed out at 220K. However the PL2 is annealed only by 40~50% at the same temperature. Thus the PL2 centers and the optically induced absorption centers are different centers.

Next we will see the isochronal annealing behavior of the fatigue of the PL1. We made two kinds of measurements with different band-gap irradiation conditions: one is a weak irradiation condition, that is, the irradiation intensity is 40mW/cm<sup>2</sup> and the irradiation time is 10s, and the other is strong irradiation condition, that is, the irradiation intensity is 300mW/cm<sup>2</sup> and the irradiation time is an hour. The strong irradiation condition is the same as that for the PL2 and the optically induced absorption.  $\Delta I/\Delta I_0$  is plotted as a function of annealing temperature  $T$ , where  $\Delta I$  is the difference between the PL intensity before fatigue and that after fatigue.  $\Delta I_0$  is the initial difference ( $T=4.2K$ ). The PL1 fatigue due to weak and short time irradiation, which is denoted as (●) in fig.4.8, is almost annealed out at 220K and this annealing behavior is similar to that of the optically induced absorption. The fatigue by the strong irradiation, which is denoted as (□) in the figure, is annealed by about 40% at 220K and

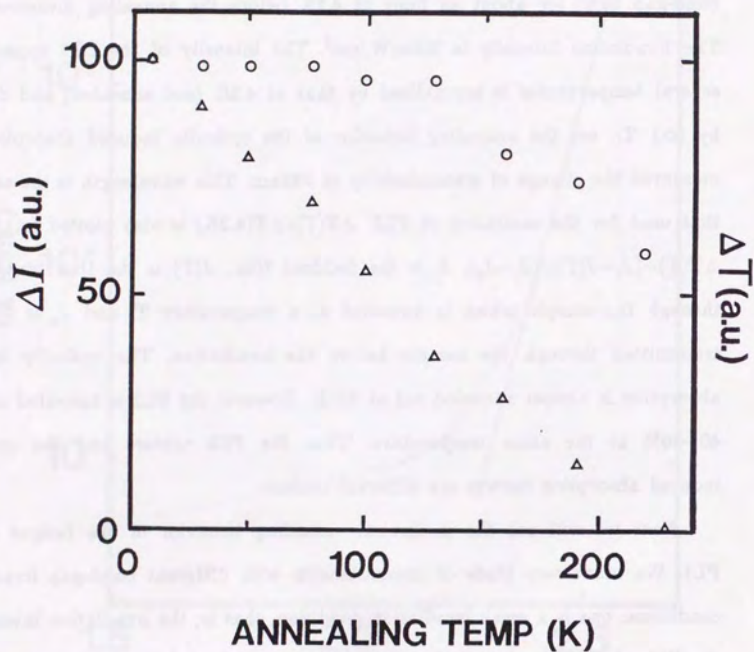


Figure 4.7

The results of isochronal annealing of PL2 (○) and the optically induced absorption (△) are shown. The measurements were carried out at 4.2K after the sample was warmed up to a chosen annealing temperature and re-cooled. The total PL intensity was monitored.

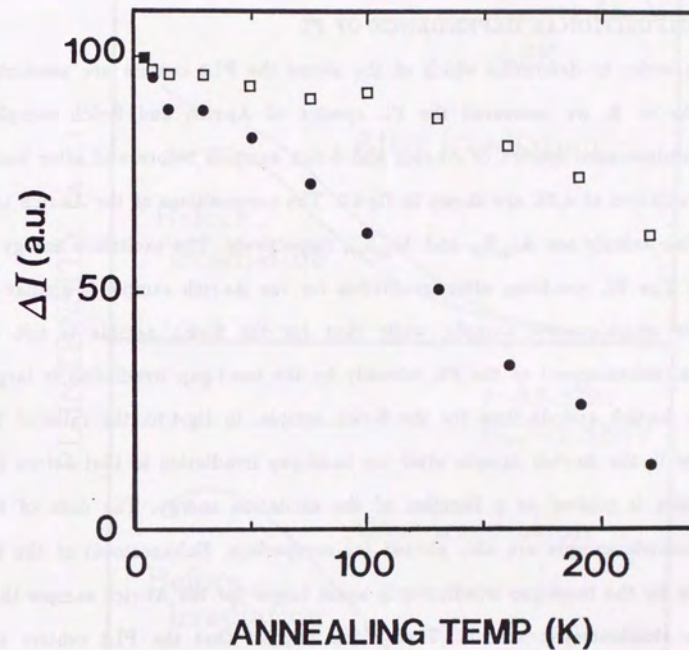


Figure 4.8

The results of isochronal annealing of PL1 fatigue are shown. (●) and (□) correspond to the short-time and long-time band-gap irradiation. The detected emission energy was 1.1eV.

this is similar to the annealing behavior of the PL2 centers with the strong irradiation.

#### 4.4 COMPOSITIONAL DEPENDENCE OF PL

In order to determine which of the atoms the PL2 centers are associated with, As or S, we measured the PL spectra of As-rich and S-rich samples. Photoluminescence spectra of As-rich and S-rich samples before and after band-gap irradiation at 4.2K are shown in fig.4.9. The compositions of the As-rich and the S-rich sample are  $As_{43}S_{57}$  and  $As_{33}S_{67}$ , respectively. The excitation energy is 1.58eV. The PL spectrum after irradiation for the As-rich sample is similar to that for stoichiometric sample, while that for the S-rich sample is not. In addition, enhancement of the PL intensity by the band-gap irradiation is larger for the As-rich sample than for the S-rich sample. In fig.4.10, the ratio of PL intensity in the As-rich sample after the band-gap irradiation to that before the irradiation is plotted as a function of the excitation energy. The data of the stoichiometric sample are also plotted for comparison. Enhancement of the PL intensity by the band-gap irradiation is again larger for the As-rich sample than for the stoichiometric sample. These facts suggest that the PL2 centers are associated with the As atoms.

#### 4.5 THERMAL QUENCHING OF PL

The temperature dependence of PL2 is plotted in fig.4.11. Since the PL2 centers are annealed by raising the temperature, we always measured the PL intensity at 4.2K after every measurement at  $T$  and corrected the annealed results by dividing the PL intensity at  $T$  by that at 4.2K. At temperatures higher than 50K, the temperature dependence can be described by equation (2.2.2). The excitation energy was 1.58eV. From equation (2.2.4),  $p_{nr}$  can be written as

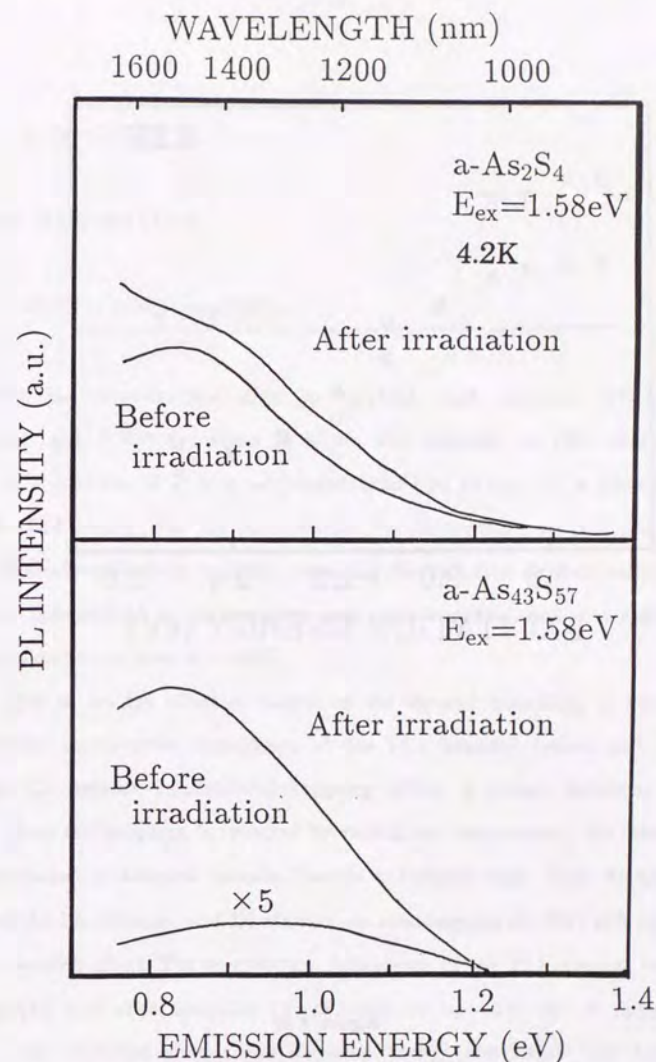


Figure 4.9

PL spectra of (a) a S-rich sample and (b) an As-rich sample are shown. The excitation energy is 1.58eV. Irradiation energy is 2.41eV for the S-rich sample and 2.35eV for the As-rich sample.

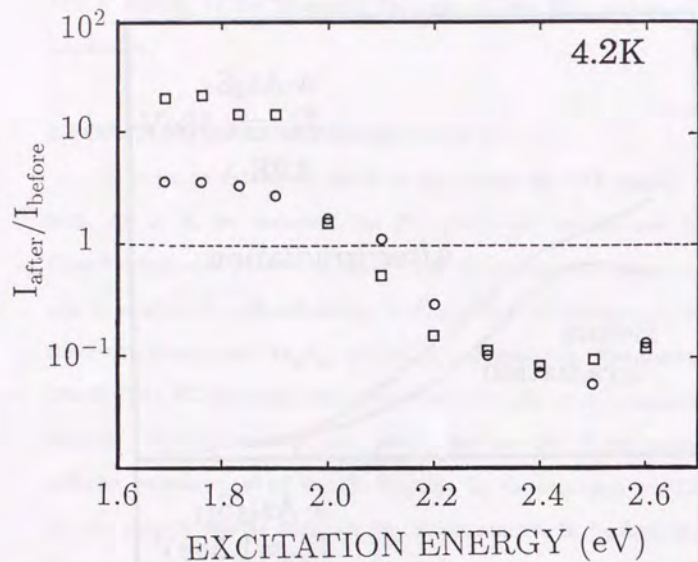


Figure 4.10

The ratio of PL intensity after band-gap irradiation to that before the irradiation is plotted as a function of excitation energy for the As-rich sample ( $\square$ ) and the stoichiometric sample ( $\circ$ ). The detected emission energy was 0.82eV.

$$p_{\text{nr}}/p_r = G/I(T) - 1, \quad (4.5.1)$$

Thus from (2.2.3) and (4.5.1),

$$G/I(T) - 1 = W_0/p_r \exp(T/T_0). \quad (4.5.2)$$

We fitted the experimental data to eq.(4.5.2) and obtained  $G/I_0=1.35$ ,  $W_0/p_r=0.24$ , and  $T_0=30(\text{K})$ , where  $I_0$  is the PL2 intensity at 4.2K.  $G/I-1$  is plotted as a function of  $T$  in a semi-logarithmic plot in fig.4.12. A good fit is obtained. This shows that the non-radiative recombination rate for the PL2 centers is well-described by eq.(2.2.4), assuming the radiative recombination rate is almost independent of temperature, and thus suggests that non-radiative recombination occurs even at  $T=0(\text{K})$ .

In order to see the effect of fatigue on the thermal quenching of PL1, we observed the temperature dependence of the PL1 intensity before and after fatiguing. To prevent unintentional fatiguing effect, a pulsed technique was utilized. Since the fatiguing is reversed by raising the temperature, the intensity is less quenched in fatigued samples than in unfatigued ones. Thus we always measured the PL intensity at 4.2K after every measurement at  $T(\text{K})$  and correct for the reversing effect. The temperature dependence of the PL1 intensity before fatiguing ( $\circ$ ) and after fatiguing ( $\Delta$ ) is fitted by eq.(4.5.2) and is shown in fig.4.13. The excitation energy and detection energy are 2.41eV and 1.24eV, respectively. The fitting parameters used for the unfatigued sample are  $G/I_0=1.9$ ,  $W_0/p_r=0.42$ , and  $T_0=20\text{K}$ . Those of the fatigued samples are  $G/I_0=2.5$ ,  $W_0/p_r=0.73$ , and  $T_0=22\text{K}$ . The fatiguing has only a little effect on the thermal quenching of PL1.

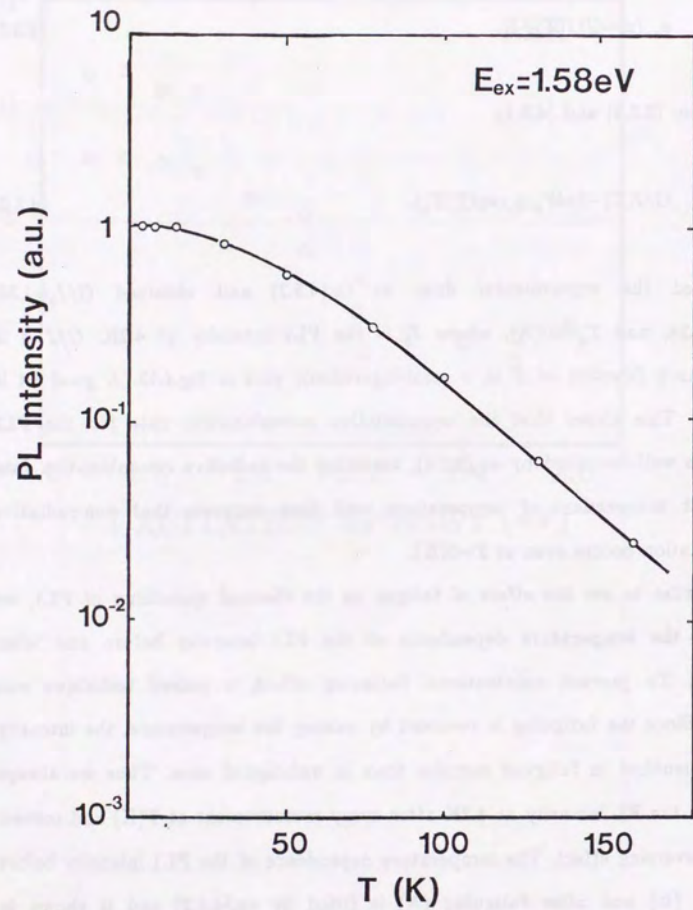


Figure 4.11

The temperature dependence of the total PL2 intensity.

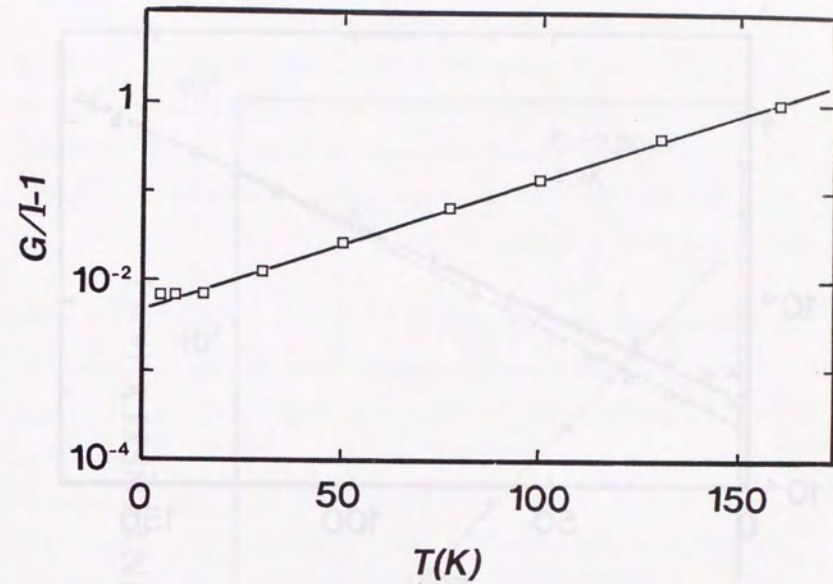


Figure 4.12

$G/I-1$  is plotted as a function of temperature, where  $I$  is the total PL2 intensity and  $G$  is the fitting parameter described in eq.(4.5.1) in the text, which corresponds to the generation rate. The solid line is the result of fitting.

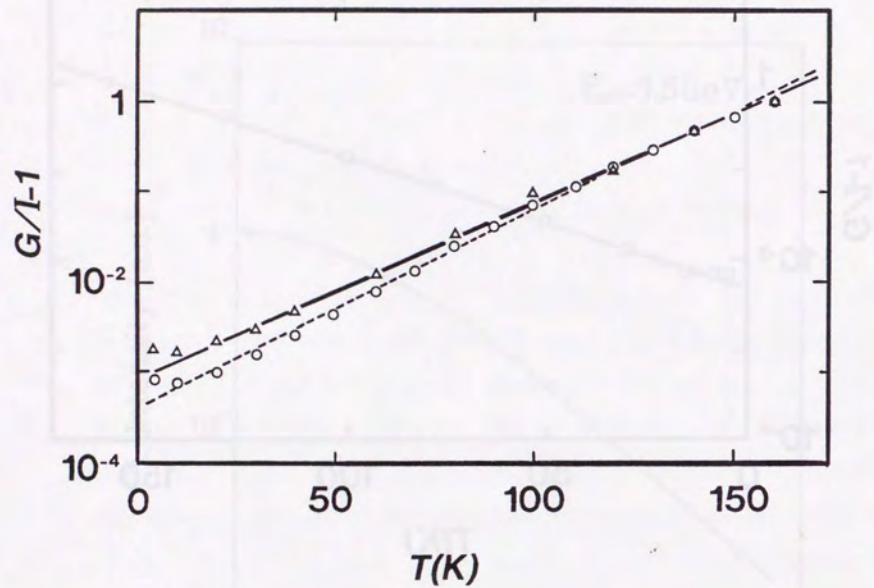
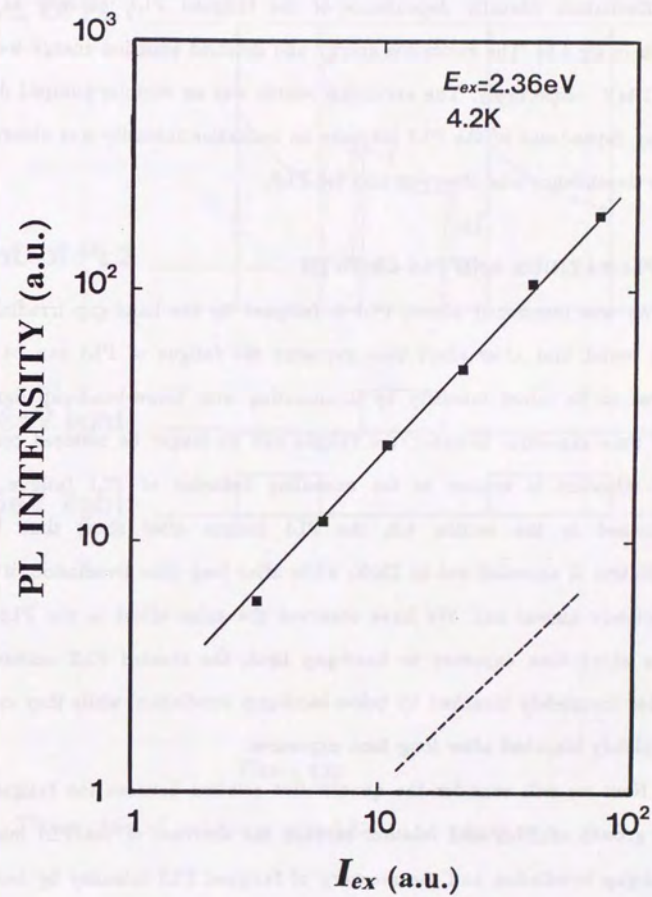


Figure 4.13

$G/I-1$  for PL1 before( $\circ$ ) and after fatigue ( $\Delta$ ) is plotted as a function of temperature, where  $I$  is the PL1 intensity and  $G$  is the fitting parameter described in eq.(4.5.1) in the text, which corresponds to the generation rate. The solid line is the result of fitting for the data after band-gap irradiation and the dashed line for the data before band-gap irradiation. The detected emission energy was 1.2eV.



#### 4.6 EXCITATION INTENSITY DEPENDENCE

Excitation intensity dependence of the fatigued PL1 intensity at 4.2K is shown in fig.4.14. The excitation energy and detected emission energy were 2.3eV and 1.1eV, respectively. The excitation source was an excimer-pumped dye laser. Linear dependence of the PL1 intensity on excitation intensity was observed. The same dependence was observed also for PL2.

#### 4.7 PL1 FATIGUE AND PL2 GROWTH

As was mentioned above, PL1 is fatigued by the band-gap irradiation. We have found that after short time exposure the fatigue of PL1 can be restored almost to its initial intensity by illuminating with below-band-gap light. After long time exposure, however, the fatigue can no longer be restored completely. This situation is similar to the annealing behavior of PL1 fatigue. As was mentioned in the section 4.3, the PL1 fatigue after short time band-gap irradiation is annealed out at 220K, while after long time irradiation, it does not completely anneal out. We have observed the same effect in the PL2 centers. After short time exposure to band-gap light, the created PL2 centers can be almost completely bleached by below-band-gap irradiation, while they can not be completely bleached after long time exposures.

Next we will consider the quantitative relation between the fatigue of PL1 and growth of PL2, and relation between the decrease of the PL1 intensity by band-gap irradiation and the recovery of fatigued PL1 intensity by below-band-gap irradiation. The sample of  $\alpha\text{-As}_2\text{S}_3$  was irradiated with 1.58eV and 2.41eV light alternately at 4.2K, and we measured PL2 and PL1 intensity. The irradiation time of the 2.41eV light was increased progressively (see fig.4.15). The irradiation time of the 1.58eV light is sufficiently long for the saturation of the bleaching of the PL2 centers and the PL1 fatigue. In fig.4.16,  $\Delta I_2$  is plotted as a function of  $\Delta I_1'$  ( ).  $\Delta I_2$  is the growth of PL2 and  $\Delta I_1'$  is the decrease

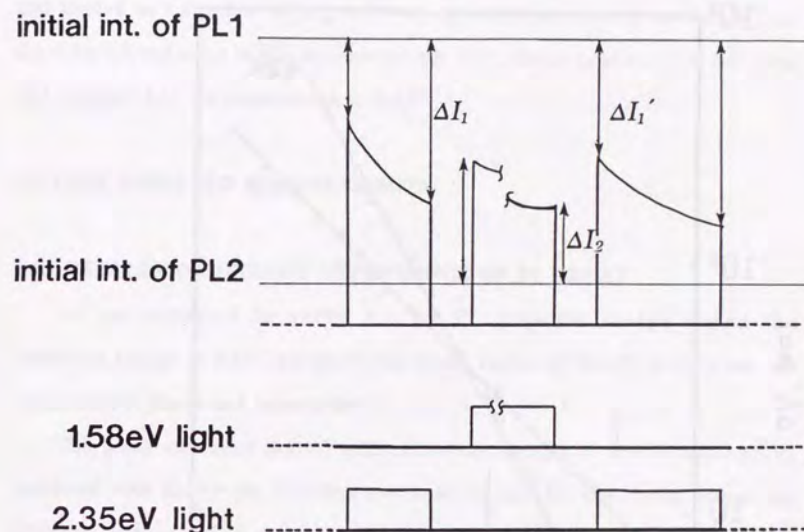


Figure 4.15

Timing chart of irradiation with 2.35eV and 1.58eV light.

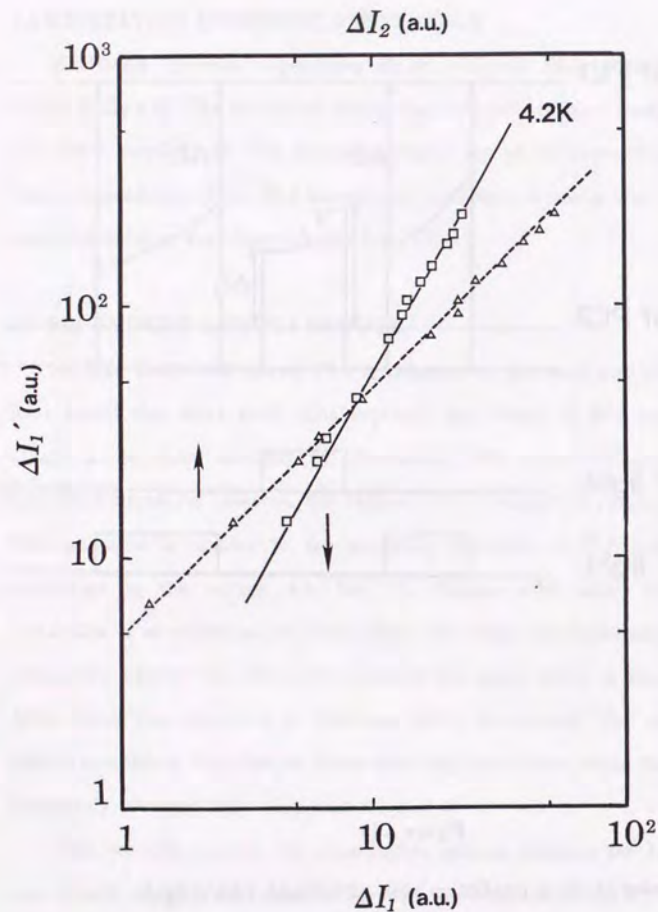


Figure 4.16

The component of PL1 fatigue that cannot be bleached by below-gap irradiation are plotted as a function of the total PL1 fatigue ( $\square$ ). The relation between the increase of PL2 intensity and the decrease of PL1 intensity is also shown ( $\Delta$ ). The detected emission energy was 0.92eV. (see fig.4.15).

of PL1 intensity (see fig.4.15).  $\Delta I_2$  is proportional to  $\Delta I_1'$ . In fig.4.16,  $\Delta I_1'$  is also plotted as a function of  $\Delta I_1$ .  $\Delta I_1'$  is the component that is not restored by the 1.58eV irradiation in the decrease of the PL1 intensity, and  $\Delta I_1$  is the total PL1 fatigue.  $\Delta I_1'$  is proportional to  $\Delta I_1^{1.8}$ .

#### 4.8 TIME RESOLVED MEASUREMENTS

##### 4.8.1 EXCITATION ENERGY DEPENDENCE OF PL DECAY

As was mentioned in section 4.2, the PL properties change around the excitation energy of 2.2eV. Similarly, the decay curves of the PL is different for the excitation above and below 2.2eV.

The decay curves of the PL with excitation energies of 1.58eV and 1.88eV, measured with the Ge-pin detector, are shown in fig.4.17. The decay curves are different between before and after the band-gap irradiation. As was mentioned in the section 4.1, this shows that the new PL centers are generated by band-gap irradiation. The PL decay in a-As<sub>2</sub>S<sub>3</sub> can be empirically fitted by the derivative of the stretched exponential function:

$$f(t) = 1/t^{1-\beta} \cdot \exp[-(t/\tau)^\beta], \quad 0 \leq \beta \leq 1. \quad (4.8.1)$$

The response time of the Ge-pin detector is about 200ns. We estimated the life times by the convolution of  $f(t)$  with the instrument function. The decay curves before the band-gap irradiation consist of two components with life times of  $10^{-6}$ s and  $10^{-4}$ s at 4.2K. The slow decay component is much weaker than the fast component. The decay curves after the band-gap irradiation, that is, the decay curves of PL2, also consist of two components, whose life-times are  $10^{-7}$ s and  $10^{-3}$ s at 4.2K.

The slow decay component of PL2 gets stronger as the excitation energy

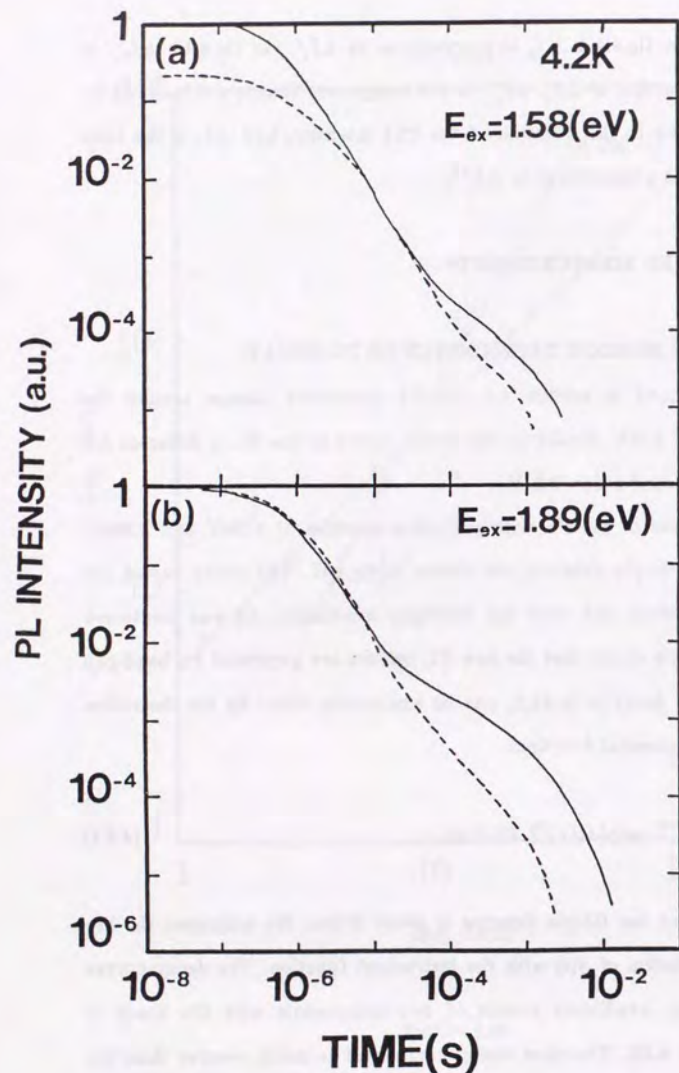


Figure 4.17

The decay curves of PL intensity with time before and after band-gap irradiation with excitation energy of (a) 1.58 eV and (b) 1.89 eV are shown. The dashed and solid lines represent the PL decay before and after the band-gap irradiation, respectively. The emitted photons of energy range from 0.7 to 1.2 eV are detected.

increases. This trend can be explored in more detail if one extracts the distribution of decay rates from the decay curves. According to Higashi and Kastner [Higashi and Kastner 1983], one can easily determine the relative number of photons emitted for any given rate in an approximate way. Consider a system experiencing a simple exponential decay for which the PL intensity is given by:

$$I(t) = N \exp(-\nu t) \tag{4.8.2}$$

where  $N$  is the number of centers initially excited and  $\nu$  is the luminescence decay rate. This equation simply states that  $I(t)$  is the number of centers surviving at time  $t$  multiplied by the probability per unit time,  $\nu$ , that these will radiate a photon. It is clear from eq.(4.8.2) that the PL intensity at a time equal to the inverse of the decay rate,  $t = \nu^{-1}$ , gives the number of initially excited PL centers,  $N = \nu^{-1} I(t = \nu^{-1})$ . From this, one can see immediately how to extract the relative number of PL centers excited if the decay rates are well separated.

This simple approach can be extended to analyze the decay exhibiting a continuous distribution of rates in the following way. The general expression for the decay is:

$$I(t) = \int N(\nu) [\nu \exp(-\nu t)] d\nu \tag{4.8.3}$$

Here,  $N(\nu)d\nu$  is the number of PL centers initially excited with rates between  $\nu$  and  $\nu + d\nu$ . The term in brackets in eq.(4.8.3) is a temporal resolution function, probing the distribution  $N(\nu)$ . This resolution function has the properties that it is peaked at  $\nu = t^{-1}$ , and that its width and magnitude are proportional to  $t^{-1}$ . Now when  $N(\nu)$  is slowly varying compared with the resolution function, eq.(4.8.3) gives

$$I(t) \sim N(\nu_t)/t^2, \quad (4.8.4)$$

where  $\nu_t = t^{-1}$ . Here we introduce the valuable  $\nu_t' = \ln \nu_t$  and the rate distribution function,  $N'(\nu_t')$ , which is defined by

$$N'(\nu_t') d\nu_t' = N(\nu_t) d\nu_t. \quad (4.8.5)$$

Since

$$\begin{aligned} N(\nu_t) &= N'(\nu_t') [d\nu_t' / d\nu_t] \\ &= t N'(\nu_t'), \end{aligned} \quad (4.8.6)$$

one has that

$$tI(t) \sim N'(\ln(\nu_t)). \quad (4.8.7)$$

Thus, from the experimental values of  $tI(t)$  one obtains  $N'(\ln(\nu))$ . Clearly, in the case of narrow distribution of rates this technique gives a result which is resolution-limited. However, if one applies this technique to a decay which is exactly exponential, one can estimate the resolution function and test whether the results are strongly affected by the finite resolution. Of course, a less approximate method would be to obtain the inverse Laplace transformation of the data, but that procedure is time-consuming and provides little additional information for systems like the chalcogenide glasses, for which the decay is found to have a relatively broad distribution of rates.

Returning to the specific case of a-As<sub>2</sub>S<sub>3</sub>, the distribution of rates extracted from the decay of PL for various excitation energies by using eq.(4.8.7) are plotted in fig.4.18. The samples had been irradiated with band-gap light for

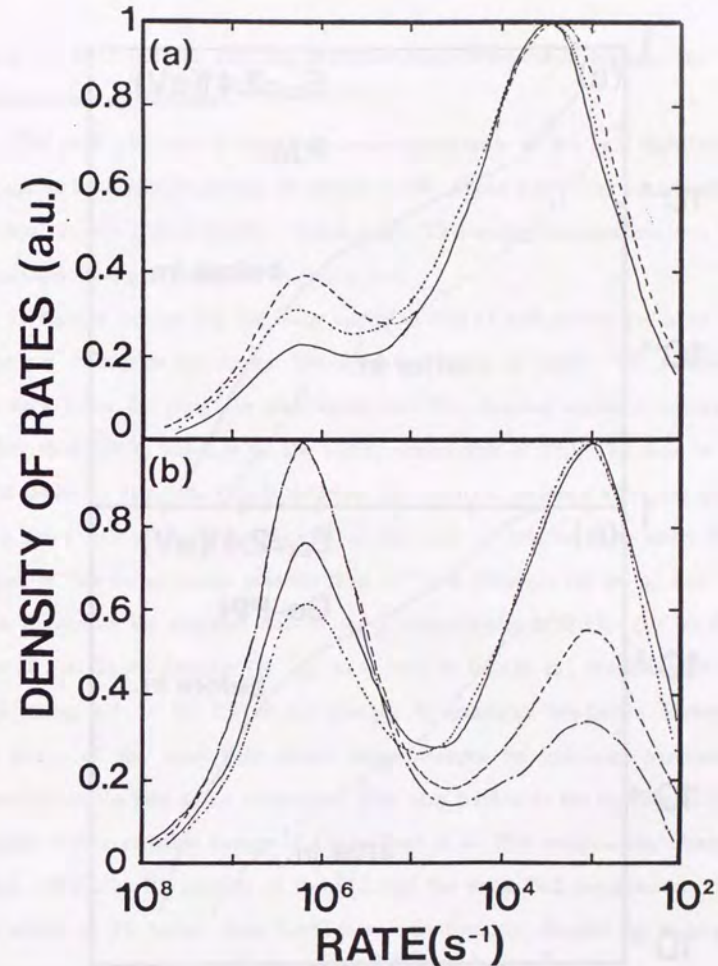


Figure 4.18

The distribution of recombination rates extracted from the PL decay. The sample had been irradiated with band-gap light. Excitation energies are (a) 2.46eV for -----, 2.32eV for ———, and 2.21eV for -·-·-·-, (b) 2.07eV for ———, 1.85eV for -----, 1.75eV for -·-·-·-, and 1.68eV for ·····.

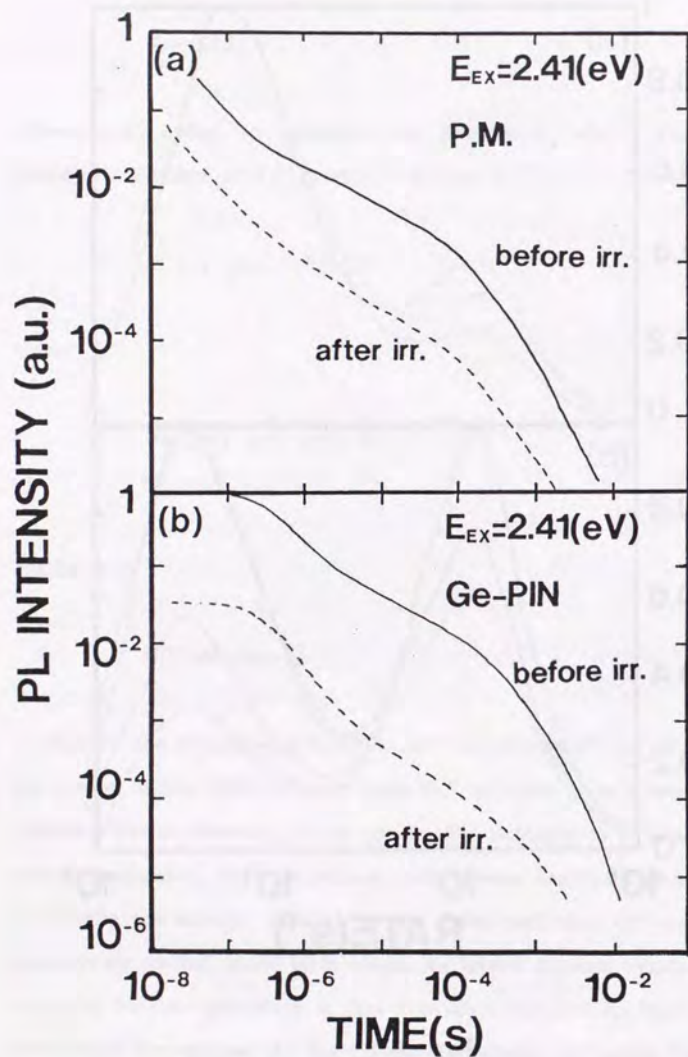


Figure 4.19

The decay curves of PL1 with time before and after fatigue. (a) The photomultiplier was used, whose response time is  $10^{-8}$ s. (b) Ge-pin detector was used, whose response time is  $10^{-7}$ s.

about an hour. As one can see, the slow decay component decreases as the excitation energy decreases.

The peak positions of the slow decay components in the rate distribution change at an excitation energy of around 2.2eV. Above 2.2eV, the peak position is about  $3 \times 10^3 s^{-1}$ . It is  $1 \times 10^3 s^{-1}$  below 2.2eV. This energy is consistent with the separation energy  $E_s$  described in section 4.2.

In fig.4.19 (a) and (b), the decay curves of PL1 at 4.2K before and after the band-gap irradiation are shown. The excitation energy is 2.41eV. The results in (a) were taken by using the photomultiplier. The detected emission energy is higher than 1.2eV, which is on the higher energy side of PL1. The data in (b) were taken by using the Ge-pin detector. The detected emission energy is lower than 1.4eV and most of the photons in PL1 can be detected. The short time region of the decay curves (shorter than  $10^{-7}$ s) is different for in (a) and (b). This is because the response time of the photomultiplier is shorter ( $10^{-8}$ s) than that of the Ge-pin detector ( $10^{-7}$ s). As is seen in fig.4.19 (a), the decay of the high energy side of the PL1 is not changed by band-gap irradiation. However, the shape of the total light decay curve changes by band-gap irradiation, especially in the fast decay component. This may be due to the creation of PL2 centers. Above emission energy of 1.2eV, there is no PL2 components. However below 1.2eV, the PL consists of the PL1 and the weak PL2 components. Thus the decay of PL higher than 1.2eV is not significantly changed by band-gap irradiation.

#### 4.8.2 TEMPERATURE DEPENDENCE OF PL2 DECAY

In fig.4.20, the decay of PL2 at 4.2K and 15K are shown. The excitation energy is 1.74eV. The life-time,  $\tau$ , of the slow decay component of PL2 is getting shorter as the temperature is raised. This behavior is empirically described by the following equation

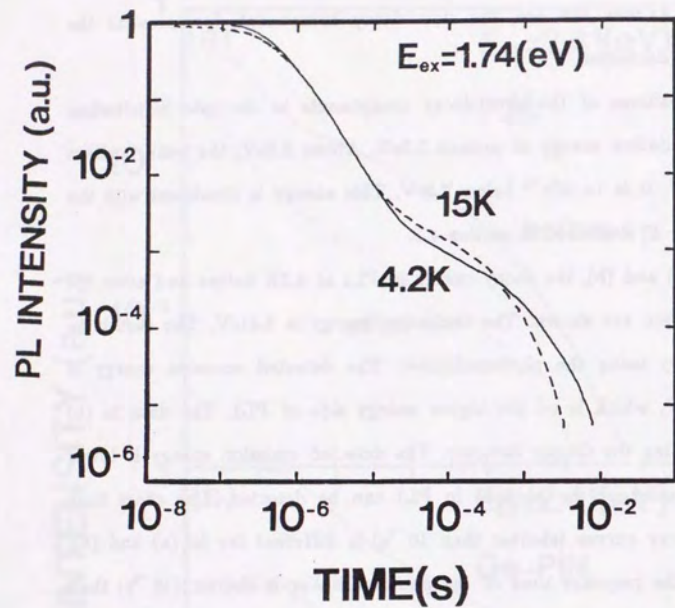


Figure 4.20

The decay curves of PL2 intensity with time at 4.2K and 15K. The excitation energy is 1.74eV. The emitted photons of energy range from 0.7 to 1.2eV are detected.

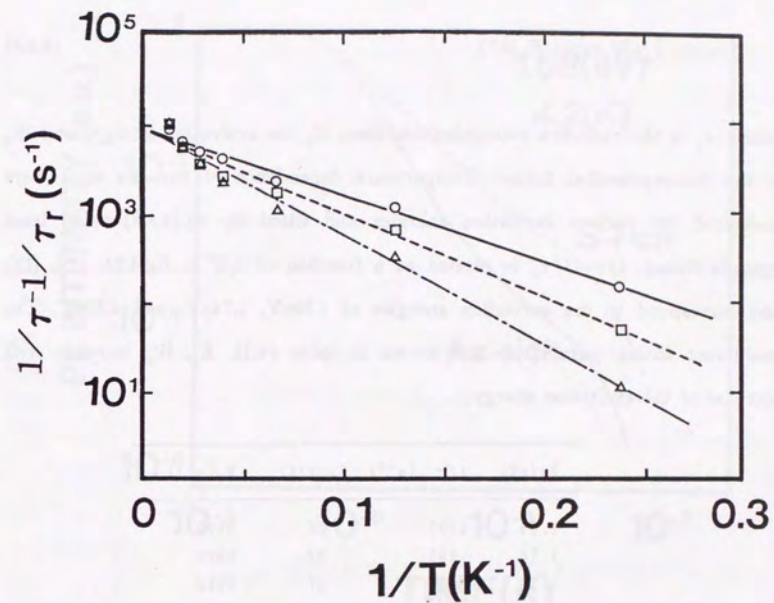


Figure 4.21

The temperature dependence of lifetimes ( $\tau$ ) of PL.  $1/\tau - 1/\tau_r$  is plotted as a function of inverse of temperature.  $\tau_r$  is the fitting parameter corresponding to radiative recombination time. The excitation energies are 1.59eV ( $\circ$ ), 1.74eV ( $\square$ ), and 1.89eV ( $\Delta$ ). The lines are the results of the fitting.

$$1/\tau = 1/\tau_r + W_0 \exp(-E_0/kT), \quad (4.8.8)$$

where  $\tau_r$  is the radiative recombination time,  $E_0$  the activation energy, and  $W_0$  is the pre-exponential factor. Temperature dependence of the life time were measured for various excitation energies and fitted by eq.(4.8.8) using least squares fitting.  $1/\tau - 1/\tau_r$  is plotted as a function of  $1/T$  in fig.4.21. (O), ( $\square$ ), ( $\Delta$ ) correspond to the excitation energies of 1.59eV, 1.74eV, and 1.89eV. The calculated fitting parameters are shown in table (4.1).  $E_0$ ,  $W_0$  increase with increase of the excitation energy.

Ex (eV)	$1/\tau_r$ (s <sup>-1</sup> )	$E_0/k$ (K)	$W_0$ (s <sup>-1</sup> )
1.89	1100	28	9500
1.74	860	22	8600
1.59	1860	17	8000

Table 4.1

#### 4.8.3 COMPOSITIONAL DEPENDENCE OF DECAY

The shapes of the decay curves for the As-rich and the S-rich samples are altered by the band-gap irradiation. In fig.4.22, the decay curves of the PL with excitation energy of 1.69eV for the S-rich (a-As<sub>3</sub>S<sub>7</sub>) and the As-rich (a-As<sub>43</sub>S<sub>57</sub>) samples after the band-gap irradiation are shown. The slope of the decay of the fast component for the S-rich sample after the band-gap irradiation are quite different from that of the PL2 decay of the stoichiometric sample, while that for the As-rich sample is similar. This suggests that the PL2 centers are associated with the As atoms.

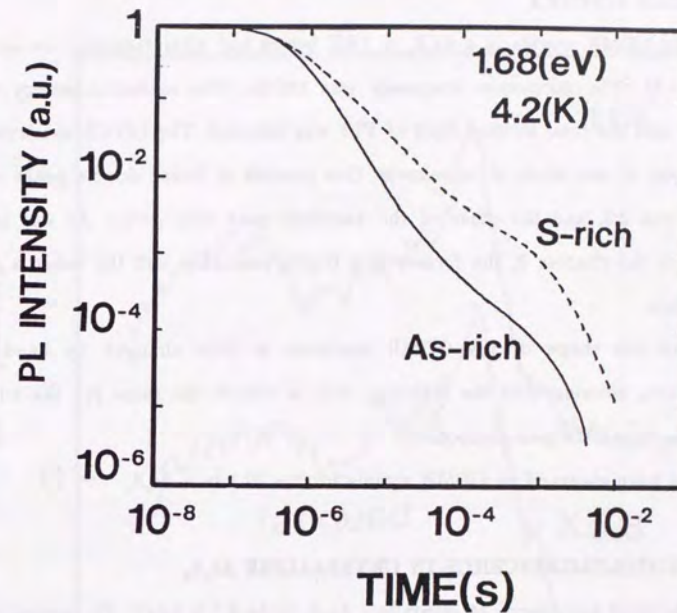


Figure 4.22

The decay curves of PL with time for S-rich sample and As-rich sample. The samples were irradiated with band-gap light before the measurement. The solid line for As-rich sample and the dashed line for S-rich sample. The emitted photons of energy range from 0.7 to 1.2eV are detected.

#### 4.9 ODMR SPECTRA

The ODMR spectra in  $a\text{-As}_2\text{S}_3$  at 1.6K before and after fatiguing are shown in fig.4.23. The microwave frequency was 25GHz. The excitation energy was 2.41eV and the total emitted light of PL1 was detected. The ODMR spectrum is composed of two kinds of resonances: One consists of broad double peaks with  $g=6.0$  and 2.3, and the other of the narrower peak with  $g=2.0$ . As was mentioned in the chapter 2, the former is a triplet resonance and the latter a pair resonance.

The line shape of the ODMR spectrum is little changed by band-gap irradiation, showing that the fatiguing rate is almost the same for the triplet component and the pair component.

We have observed no ODMR signals for the PL2 in  $a\text{-As}_2\text{S}_3$ .

#### 4.10 PHOTOLUMINESCENCE IN CRYSTALLINE $\text{As}_2\text{S}_3$

The band gap energy of crystalline  $\text{As}_2\text{S}_3$  ( $c\text{-As}_2\text{S}_3$ ) is 2.6eV. PL spectra with band-to-band excitations are shown in fig.4.24 (a). The excitation energy is 2.71eV. The peak energy is 1.24eV. This PL spectrum is consistent with the PL spectra of  $c\text{-As}_2\text{S}_3$  reported by many authors [Kolomiets *et al.* 1970, Murayama *et al* 1981]. The fatiguing effect is weak for this PL. We observed that the PL intensity was reduced to about a half of the initial intensity by the band-gap irradiation. In fig.4.24 (b), the PL spectra with excitation energy of 2.41eV are shown. The peak energy is 1.08eV. This PL spectrum is very similar to PL1 in the amorphous sample and also has the strong fatiguing effect. The PL intensity was reduced to about one tenth of the initial intensity by the irradiation of 2.41eV light, while the intensity of the PL with band-to-band excitation was reduced little by this irradiation (see fig.4.24(a)).

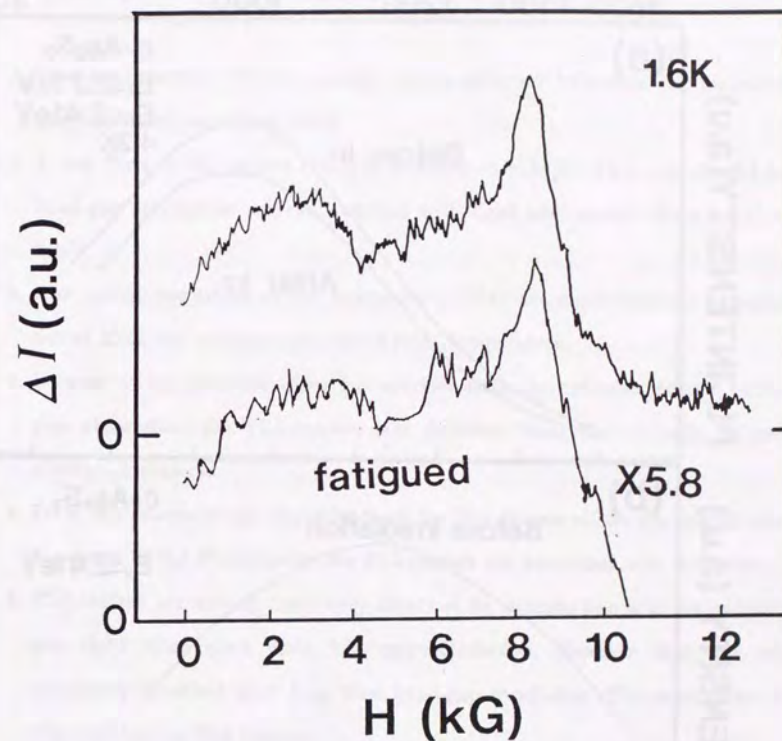


Figure 4.23

The ODMR spectra of  $a\text{-As}_2\text{S}_3$  at 2K before and after fatigue. The excitation energy is 2.41eV.

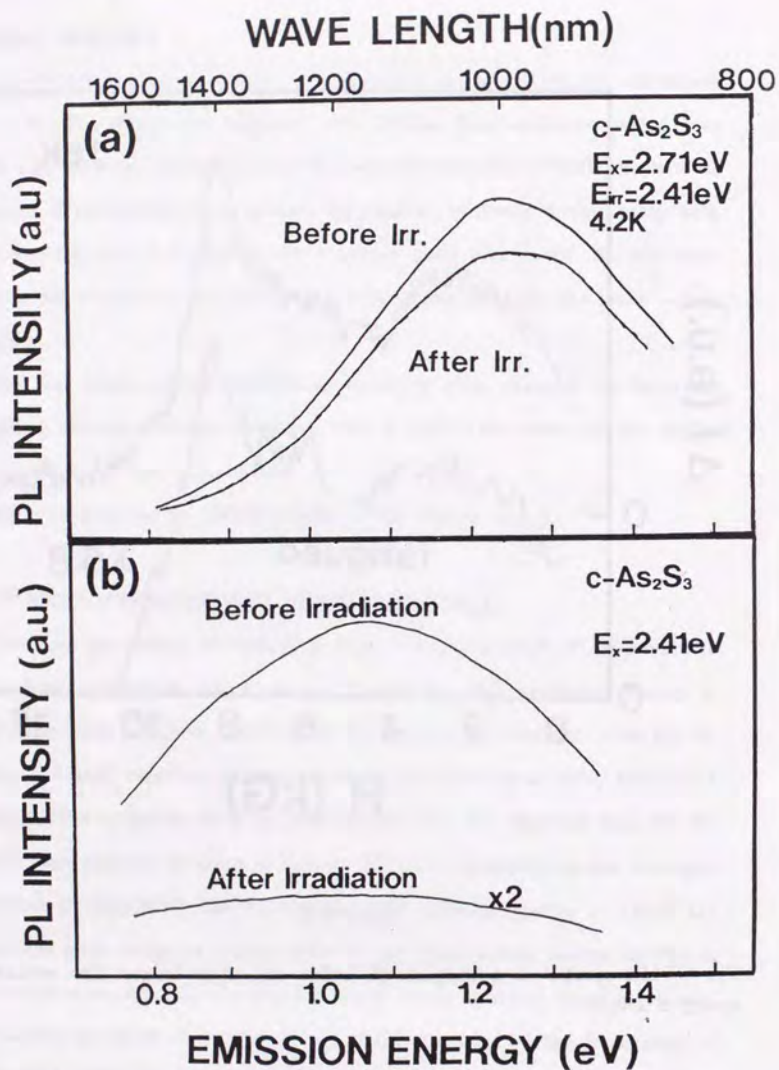


Figure 4.24

PL spectra of  $c\text{-As}_2\text{S}_3$  before and after irradiation of 2.41eV light. The excitation energies are (a) 2.71eV and (b) 2.41eV.

#### 4.11 SUMMARY OF EXPERIMENTAL RESULTS

The experimental results are summarized as follows:

1. Photoluminescence (PL) in  $a\text{-As}_2\text{S}_3$  shows different behaviors for excitation energies below and above 2.2eV.
2. A new kind of PL centers (PL2) is observed in  $a\text{-As}_2\text{S}_3$ . They are created by band-gap irradiation and well excited with light with energy from 1.4eV to 2.2eV.
3. PL2 centers are stable at low temperature. They are not completely annealed out at 220K but are annealed out at room temperature.
4. Because of the different annealing behavior from the optically induced below-gap absorption, the PL2 centers are different from the optically induced absorption centers.
5. From the compositional dependence of the line shapes of the PL spectra and the decay of the PL intensity, the PL2 centers are associated with As atoms.
6. PL2 centers are almost completely bleached by illuminating with below-band-gap light after short time band-gap irradiation. However they are not completely bleached after long time band-gap irradiation. The same effect is observed for the PL1 fatigue.
7. The temperature dependence of PL2 intensity is described as  $I=I_0\exp(-T/T_0)$ .
8. The excitation intensity dependence of the fatigued PL1 intensity is linear.
9. The decay of PL2 consists of the two components, the slow decay component and the fast decay component. They are empirically fitted by the derivative of the stretched exponential function, and their life-times are  $10^{-7}$  for the fast decay component and  $10^{-3}$  for the slow.
10. Relative intensity of the slow decay component in PL2 increases as excitation energy increases.

11. The life time of the slow decay component decreases as temperature rises. This behavior can be described by an activation process.
12. The annealing behavior of the PL1 fatigue depends on the irradiation condition. After short-time irradiation, it is similar to that of the optically induced absorption band and annealed out at 220K. However it is different after long-time band-gap irradiation. It is not completely annealed out until annealing temperature gets to room temperature.
13. The line shape of ODMR in PL1 dose not significantly changes after fatigue.
14. We have observed new PL centers in  $c\text{-As}_2\text{S}_3$  which is similar to the PL1 centers in  $a\text{-As}_2\text{S}_3$ . The excitation energy is 2.41eV, which is lower than the band gap energy. They are strongly fatigued by irradiation of the 2.41eV light.
15. PL with band-to-band excitation in  $c\text{-As}_2\text{S}_3$  is little fatigued by the irradiation of 2.41eV light.

## Chapter 5

### Discussion

#### 5.1 PHOTOLUMINESCENCE FATIGUE

The mechanism of PL fatigue has been controversial, as it has been mentioned in chapter 2. In this section, we will discuss the mechanism of the PL fatigue. There are two candidates for reduction of the PL intensity due to the band-gap irradiation. One is the destruction of the PL centers, and the other is the enhancement of the non-radiative recombination rates.

We first consider the latter case. If carrier-carrier scattering plays an important role in the non-radiative recombination process after fatigue, the non-radiative rates are proportional to the carrier concentration. It is expected that the PL intensity is proportional to the square root of excitation intensity when this process is dominant. However, the fatigued PL1 intensity is proportional to the excitation intensity in  $a\text{-As}_2\text{S}_3$ . Therefore, interaction between the photogenerated carriers is not probable for the non-radiative processes in fatigued samples.

If the escape rates of the carriers from the PL1 centers are enhanced by band-gap irradiation, the life time of PL1 is reduced after fatigue. However the PL1 decay dose not become faster after the band-gap irradiation as is seen in fig.4.19 (a).

The measurement of thermal quenching of PL1 intensity gives  $W_0/p_r=0.42$  for the unfatigued sample and  $W_0/p_r=0.73$  for the fatigued sample, as was mentioned in section 4.5. The non-radiative rate becomes a little faster after fatigue. The band-gap irradiation reduces the PL intensity to less than one tenth of the initial intensity although the non-radiative rate becomes only 1.7 times larger. Thus the reduction of the PL1 intensity cannot be explained solely by the

enhancement of the non-radiative rate.

These facts suggest that shortly after the pulsed excitation (at least shorter than  $10^{-8}$  sec, which is the time-resolution of our detection system), the carriers are already determined to recombine radiatively or non-radiatively. The cause of the PL fatigue is the reduction in the relative number of carriers which are captured by the PL centers. In order to examine whether this is due to an enhancement of the nonradiative centers or a reduction of the radiative centers, we will study the PL centers in  $c\text{-As}_2\text{S}_3$ , which has similar PL to that of the amorphous phase.

In  $c\text{-As}_2\text{S}_3$ , PL excited with 2.41eV light is similar to the PL1 in  $a\text{-As}_2\text{S}_3$ . This PL is exhaustively fatigued by irradiation of 2.41eV light. It is impossible to obtain synthetic crystals and the crystalline  $\text{As}_2\text{S}_3$  is a natural orpiment. Therefore the sample may contain a lot of structural defects similar to those in amorphous samples. The ODMR spectrum in  $c\text{-As}_2\text{S}_3$  with excitation energy of 2.41eV is similar to that in  $a\text{-As}_2\text{S}_3$  [Suzuki 1982]. Also in  $c\text{-As}_2\text{Se}_3$ , the ODMR spectra with the excitation energy lower than the band-gap energy are similar to those in  $a\text{-As}_2\text{Se}_3$  [Depinna and Cavenett 1982b]. If the fatigue mechanism in the crystalline samples is the same as that in amorphous samples, it is suggested that the fatigue is caused by the destruction of PL centers. The band-gap energy in  $c\text{-As}_2\text{S}_3$  is 2.6eV. Therefore the carriers are excited to the band tail states with 2.41eV light, and the extent of the wavefunction is not large. Even if non-radiative recombination centers are created by 2.41eV irradiation, the capture rates of non-radiative center are not significantly enhanced because of a low carrier mobility in the band tail. Furthermore the intensity of the intrinsic PL is not fatigued by irradiation with 2.41eV light. If the irradiation of 2.41eV light causes non-radiative centers, the intensity of the intrinsic PL should be also fatigued. However this is not the case. Thus the fatigue is caused by the destruction of the radiative recombination centers rather than the creation of

non-radiative centers.

### 5.1.1 IRRADIATION TIME DEPENDENCE OF FATIGUE

The temporal evolution of PL fatigue cannot be described by simple exponential decay functions, which suggests the broad distribution of fatigue cross section. Thus we cannot extract useful information directly from the temporal evolution.

The stability of PL1 fatigue is dependent on the irradiation time. After short-time irradiation, the fatigue is almost completely annealed out at 220K. It is also bleached by below-gap irradiation. After long time irradiation, however, PL1 fatigue is not completely bleached by annealing at 220K nor by below-gap irradiation. These facts suggest that the long time exposure to band-gap light stabilizes the fatigued PL1 centers. The previous report by Bishop *et al.* [1977b] that the LESR, the optically induced below-gap absorption, and the PL fatigue in chalcogenide glasses have similar annealing properties may correspond to the short time irradiation condition.

As was mentioned in section 4.7, the component that is not restored by the below-gap irradiation ( $\Delta I_1'$ ) is proportional to  $\Delta I_1^{1.8}$ , where  $\Delta I_1$  is the total reduction of PL1.  $\Delta I_1'$  is nearly proportional to the square of  $\Delta I_1$ . This suggests that the PL1 sites which are attacked by photo-excited carriers (or photons) twice or more times become stable fatigued sites, while those attacked only once are bleached by annealing at 220K or by below-gap irradiation.

We will consider a simple model to explain the relation between  $\Delta I_1'$  and  $\Delta I_1$ . Consider a system that has  $N$  lattice sites,  $n_1$  of which are PL1 centers. We put  $n_c$  carriers on the lattice sites randomly. The average number of PL1 centers that do not capture any carriers,  $N_0$ , is

$$N_0 = n_1(1 - 1/N)^{n_c}. \quad (5.1.1)$$

The average number of the PL1 centers that capture only one carrier,  $N_1$ , is

$$N_1 = n_1 n_c (1 - 1/N)^{n_c - 1} / N. \quad (5.1.2)$$

For  $N, n_c \gg 1$ ,

$$\approx n_1 n_c (1 - n_c/N) / N. \quad (5.1.3)$$

Thus the average number of PL1 centers that capture equal to or more than one carrier  $N_1'$  is

$$N_1' = n_1 - n_1 (1 - 1/N)^{n_c} \approx n_1 n_c / N. \quad (5.1.4)$$

The average number of PL1 centers that capture equal to or more than two carriers  $N_2$  is

$$N_2 = n_1 - n_1 (1 - 1/N)^{n_c} - n_1 n_c / N (1 - 1/N)^{n_c - 1} \\ \approx n_1 n_c^2 / N^2 \quad (5.1.5)$$

$N_1$  and  $N_2$  correspond to  $I_1, I_1'$ , respectively. Since  $n_1$  and  $N$  are constant, equations (5.1.4) and (5.1.5) shows that  $N_2$  is proportional to the square of  $N_1$ , and that  $I_1'$  is proportional to the square of  $I_1$ .

## 5.2 THE PL2 CENTERS

The annealing behavior of the PL2 centers shows that they are different from the optically induced absorption centers although the excitation spectrum

of the PL2 appears to correspond to the induced absorption band. The PL2 centers with prolonged irradiation are not annealed out until reaching room temperature.

Recently Hautala *et al.* [1988] found that there are four different kinds of light induced ESR (LESR) centers. Two kinds of the centers are annealed out at 180K. The other two kinds of the centers, however, are not annealed out until reaching room temperature. The ESR sites which anneal at lower temperatures are labeled type I sites, and there are two components to these sites, one associated with S and one with As. The sites which are thermally more stable are denoted as type II sites, which are not completely annealed out until reaching room temperature (fig.5.1). There are also two components to these sites, one associated with S and one with As, which will be denoted as  $S_{II}$  and  $As_{II}$ , respectively. The relative intensity of the type I resonance compared to the type II intensity is slightly stronger at short irradiation time. The  $S_{II}$  signals are not observed in As-rich samples and  $As_{II}$  signals are strong in As-rich samples, while  $As_{II}$  signals are not observed and  $S_{II}$  signals are strong in S-rich samples. They suggested that the  $As_{II}$  centers and the  $S_{II}$  centers are associated with As-As and S-S bonds, respectively.

Our results of the isochronal annealing is similar to the type II LESR centers observed by Hautala *et al.* This suggests that the centers of the PL2 correspond to the type II.

The PL2 is not observed in the S-rich samples but is observed in the As-rich samples. In the S-rich samples, band-gap irradiation changes the PL spectra excited with below-gap light. However the PL intensity is enhanced a little and the peak energy is below 0.8eV after the irradiation. Apparently this PL center is not the same as the PL2 centers, since the peak energy and the decay of the PL intensity are different from those of PL2. Our experimental system can not deal with emission energy below 0.8eV. Therefore we will not mention the PL

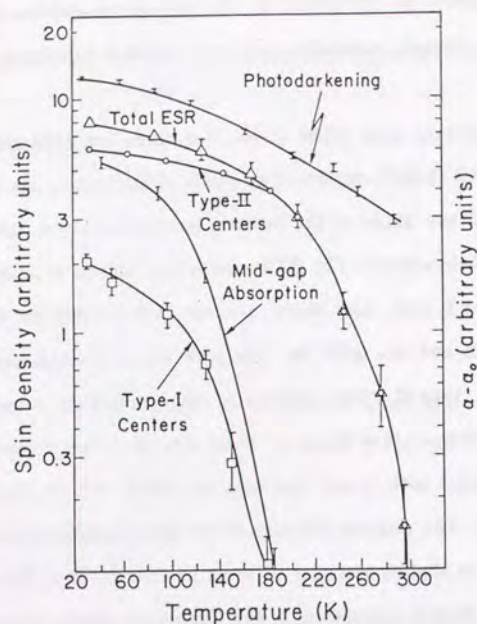


Figure 5.1

Comparison of thermal decay of the optically induced ESR, photodarkening, and mid-gap absorption in  $a\text{-As}_2\text{S}_3$ . The top (photodarkening) and middle curves (mid-gap absorption) represent the thermal annealing of the change in average absorption coefficient  $\alpha - \alpha_0$  at 2.41 and 1.30eV, respectively after irradiation at 2.41eV with about  $250\text{mW}/\text{cm}^2$  for 180min at 30K (right hand scale). The data represent  $\alpha - \alpha_0$  observed at 30K after isochronal annealing for about 10min at the indicated temperature. The other three curves represents the density of optically induced ESR with the same conditions as describes above for photodarkening. Triangles represent the total ESR intensity. Circles represent the contribution of type II centers ( $\text{As}_{\text{II}}$  and  $\text{S}_{\text{II}}$ ). Squares represent the contribution of type I centers ( $\text{As}_{\text{I}}$  and  $\text{S}_{\text{I}}$ ). The relative spin densities of the different centers are presented. [Hautala *et al.* 1988].

centers in the S-rich samples further.

The difference between the S-rich and the As-rich samples is in the amount of As-As bonds. The relative portions of As-As and S-S bonds depend dramatically on the glass composition. In the As-rich sample, there are a large number of As-As bonds, while there are no As-As bonds in the S-rich samples, which was confirmed by many authors using Raman scattering technique [Ewen *et al.* 1977, Lucovsky *et al.* 1977, Nemanich *et al.* 1978]. We believe that this strong dependence on composition is the reason for the difference between Fig.4.9 (a) and (b).

There are As-As bonds also in the stoichiometric samples. Raman scattering studies have identified the presence of "like-atom" bonds for both arsenic and sulfur in bulk  $a\text{-As}_2\text{S}_3$  [Tanaka 1987, Kawazoe 1988]. The amount of As-As or S-S bonds present was found to be highly dependent on the glass composition with no As-As Raman peak observable in S-rich samples and no S-S Raman peak observable in the As-rich glasses. The total number of homopolar bonds was determined to be  $\sim 1\%$ , which is not the small amount for the origin of PL2 centers. Therefore the PL2 centers are associated with As-As bonds.

The annealing properties of the PL2 is similar to those of PL1 fatigue. After prolonged irradiation of band-gap light, the isochronal annealing curve of the PL2 is similar to that of the PL1 fatigue, but is different from that of the optically induced absorption. The PL2 centers are different from that of the induced absorption band, while it seems that there are close relation between the PL2 growth and the PL1 fatigue. In fact, the growth of the PL2 is proportional to the decrease of PL1. These facts suggest that the PL1 centers are converted to the PL2 centers by band-gap irradiation. However not all of the PL1 centers are converted to the PL2 centers by band-gap irradiation. The compositional dependence of the PL2 suggest that it is associated with As-As bonds, but not all of the PL1 centers are associated with As-As bonds.

The ODMR measurement shows that some of the PL1 centers are associated with As-As bonds. There are two kinds of resonances in ODMR signals of a-As<sub>2</sub>S<sub>3</sub>. One of the resonances, the pair resonance, is associated with As-As bonds. The width of the pair resonance is due to the hyper-fine interaction with As-nuclei [Tada et al. 1984]. Suzuki have shown that the pair resonance become weaker as the arsenic content decreases in a-As<sub>2</sub>S<sub>1-x</sub> [Suzuki 1982]. Therefore the fraction of the PL1 centers which contributes to the pair resonance is associated with As-As bonds. As shown in fig.4.23, the line shape of ODMR spectra do not change after fatigue, namely the fatigue rates of the triplet and the pair resonance are the same.

The PL2 growth and the PL1 decrease is complimentary. Their annealing behavior is similar to each other. The PL2 centers are associated with the As-As bonds. The pair resonance of the PL1 is associated with the As-As bonds and the fatiguing behavior is almost the same as that of the total PL1. These facts altogether suggest that the component of the PL1 which contributes to the pair resonance is converted to the PL2 centers by band-gap irradiation.

### 5.2.1 THE ENERGY LEVELS OF PL2 CENTERS

PL2 is excited with below-gap light, which shows that the energy level of PL2 centers is located in the gap. Figure 4.3 shows that the peak energy of PL2 emission is about 0.85eV and it is almost independent of the excitation energies. The excitation spectra of PL2 is nearly flat in the excitation energy range from 1.6eV to 2.2eV (fig.4.4). These facts suggest that the PL2 is caused by the excitation from a localized defect state (or extended continuous states) to extended continuous states (defect state). The electrons (or holes) excited into the continuous states relax to the edge, and recombine with the holes (electrons) at the defect level. This is illustrated in fig.5.2. The excitation spectrum of PL2 has a shoulder around the excitation energy of 1.4eV. This may be an energy

difference between the band-edge and the energy level of PL2, and it is denoted as  $E_e$  in fig.5.2.

Since the  $k$ -selection rule is not maintained in amorphous materials, the absorption coefficient,  $\alpha$ , can be written as

$$\alpha(\nu) \sim \int dE N_2(E) N_c(E+h\nu) / h\nu, \quad (5.2.1)$$

where  $N_2$  and  $N_c$  is the density of states of PL2 centers and the continuous states, respectively [Mott and Davis 1979]. The integration is over all pairs of states in the continuous states and PL2 centers separated by an energy  $h\nu$ . We assume the parabolic density of states for the continuous energy levels and  $\delta$ -function-like density of states for the energy levels of PL2 centers.

$$N_2(E) = \delta(E - E_2), \quad (5.2.2)$$

$$N_c(E) = (E - E_g)^{1/2}, \quad (5.2.3)$$

where  $E_g$  and  $E_2$  are the band-gap energy and the energy level of PL2 centers. Thus the  $\alpha(\nu)$  is

$$\alpha(\nu) \sim (h\nu - E_e)^{1/2} / h\nu, \quad (5.2.4)$$

$$E_e = E_g - E_2. \quad (5.2.5)$$

The dashed line in the fig.4.4 is the curve fitted with eq. (5.2.4) with fitting parameter  $E_e = 1.42\text{eV}$ . The observed PL intensity at  $E_{ex} = 1.35\text{eV}$  is off the fitting curve. This is because the energy distribution of PL2 centers actually have some width and is not the  $\delta$ -function or electron-phonon coupling broadens the spectrum.

The peak energy of PL2 is lower by about 0.57eV than  $E_e$ , and this is due

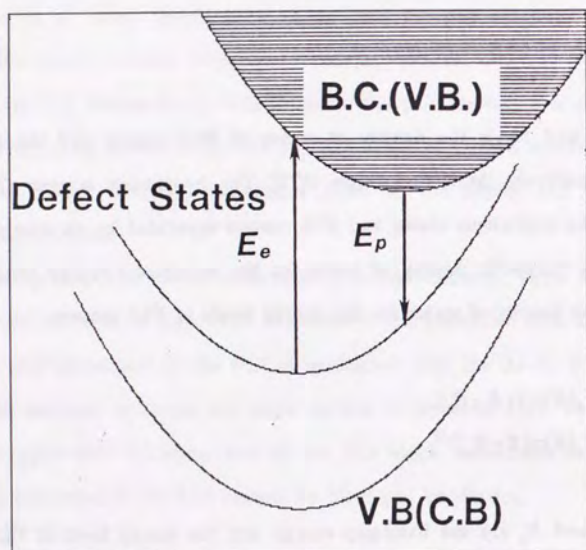


Figure 5.2

Configurational coordinate diagram of the PL2 center.

to the Stokes shift. The Stokes shift,  $2W$ , can be written as

$$2W = \delta^2 / (4 \ln(2) h \Omega), \quad (5.2.6)$$

where  $\delta$  and  $\Omega$  are the FWHM of PL2 and the vibrational frequency.  $2W$  and  $\delta$  for PL1 are about 1.2eV and 0.52eV, respectively.  $h\Omega$  is 0.081eV for PL1. Using this value for  $\Omega$  of PL2, we obtain  $2W=0.6$ eV. This is consistent with the value obtained from the excitation spectrum.

For the excitation energy higher than 2.2eV, the band-to-band excitation becomes dominant and the PL2 centers get less excited. Thus the PL2 intensity is weak for excitation energy higher than 2.2eV.

### 5.2.2 THE TEMPORAL BEHAVIOR OF PL2

The decay of the PL2 intensity after pulsed excitation consists of two components, the fast decay component and the slow decay component. The lifetimes of the fast decay component and the slow decay component are  $10^{-7}$ sec and  $10^{-3}$ sec respectively.

In a-P, a singlet exciton and a triplet exciton recombination were observed [Deppina and Cavenett 1981, Deppina *et al.* 1983]. The lifetimes of the singlet and triplet excitons are  $1.5 \times 10^{-7}$ s and  $4 \times 10^{-3}$ s, respectively. These values are very similar to those of the PL2.

The decay of the PL1 intensity of a-As<sub>2</sub>S<sub>3</sub> also has a fast and a slow decay component. The life-times of the fast and the slow decay components are  $10^{-8}$ sec and  $10^{-4}$ sec, respectively [Murayama 1983]. The fast decay component are attributed to the recombination of the singlet states. The slow decay component are attributed to the recombination of the triplet states, which was confirmed by ODMR measurements [Suzuki 1982, Tada *et al.* 1984, Depinna and Cavenett. 1982a].

Similarly, the fast and slow decay components of the PL2 are considered to be the recombination of singlet and triplet states, respectively. The life-time of the slow decay component is very large and we can consider two reasons of this long life-time. One explanation is that the distance between the electron and the hole is long and the overlap of the wavefunctions is small. The other is that the recombination process is an optically-forbidden process, that is, it is a triplet recombination process. If the triplet state were a pure triplet state, the transition from this state to the singlet ground state would be strictly forbidden, but it is weakly allowed because of spin-orbit coupling to higher-lying singlet states. The temperature dependence of the PL2 decay reveals that the latter process is more appropriate.

We will call the states that are associated with the fast and the slow decay components, respectively, the fast state and the slow states. The life time of the slow decay component of the PL2 ( $\tau$ ) gets shorter as the temperature is raised. This behavior can be described by the following equation as was mentioned in chapter 4,  $1/\tau = 1/\tau_r + W_0 \exp(-E_0/kT)$ .

There may be two interpretations of  $E_0$ . One is the activation from slow states to non-radiative recombination centers (fig.5.3 (I)). The other is activation from the slow states to the fast states (fig.5.3 (II)).

We examine both cases using simple rate equations. Although the actual decay function of the PL2 is the stretched exponential, we use exponential decay for simplicity. The rate equations of the first case are

$$dn_f/dt = -n_f/\tau_f + G_f \quad (5.2.7)$$

$$dn_s/dt = -n_s/\tau_s - n_s W_0 \exp(-E_0/kT) + G_s, \quad (5.2.8)$$

where  $n_f$  and  $n_s$  are the population of the fast and the slow states, respectively.  $\tau_f$  and  $\tau_s$  are the life-times and  $G_f$  and  $G_s$  are the generation rates. The rate

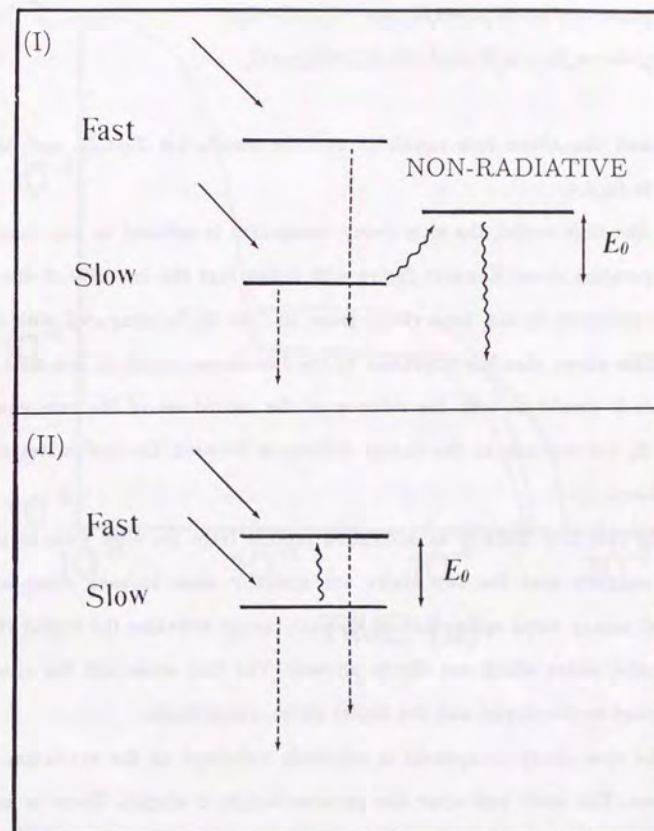


Figure 5.3

Schematic energy diagram for the fast states and slow states of the PL2 center.

equations of the second case are

$$dn_f/dt = -n_f/\tau_f - W_0 n_f + n_s W_0 \exp(-E_0/kT) + G_f, \quad (5.2.9)$$

$$dn_s/dt = -n_s/\tau_s - n_s W_0 \exp(-E_0/kT) + W_0 n_f + G_s. \quad (5.2.10)$$

We solved the above rate equations and the results for  $T=4.2\text{K}$  and  $15\text{K}$  are shown in fig.5.4.

In the first model, the slow decay component is reduced in any time range as temperature rises. However figure 4.20 shows that the intensity of the PL at  $15\text{K}$  is enhanced in the time range from  $10^{-5}$  to  $10^{-4}\text{s}$  compared with that at  $4.2\text{K}$ . This shows that the activation to the fast states occurs in this time range, and this is consistent with the solution of the second set of the rate equations. Thus,  $E_0$  corresponds to the energy difference between the fast states and the slow states.

The fact that there is an activation process from the slow state to the fast states suggests that the two states are spatially close to each other and the thermal energy turns spins, that is, thermal energy activates the triplet states to the singlet states which are dipole allowed. The fast state and the slow state correspond to the singlet and the triplet states, respectively.

The slow decay component is relatively enhanced as the excitation energy increases. The state just after the photoexcitation is singlet. There is no spin-orbit coupling between the singlet states and triplet states in the same spatial orbital. Therefore the electrons (or holes) excited with a low energy directly to the singlet recombination center can not relax to the triplet states. On the other hand, electrons excited with a higher energy have excess energy and can relax to the states with different spatial orbitals. They can then relax to the triplet states which are slightly lower in energy. Thus the slow decay component becomes relatively stronger as the excitation energy increases.

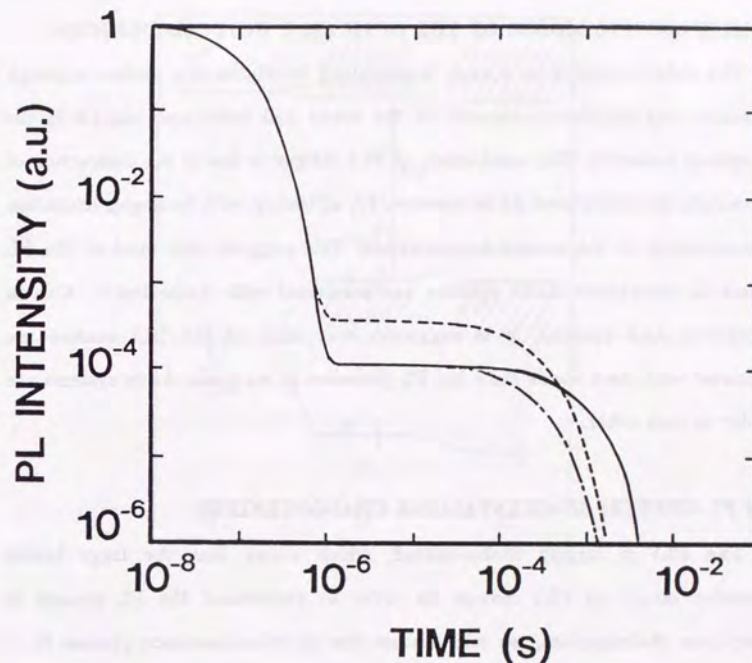


Figure 5.4

The results of simulation of the PL2 decay by using the rate equations (5.2.7)-(5.2.10). We take  $\tau_f=1 \times 10^{-7}\text{s}$ ,  $\tau_s=1 \times 10^{-3}\text{s}$ ,  $W_0=8 \times 10^3\text{s}^{-1}$ ,  $E_0/k=17\text{K}$ , and  $G_f/G_s=1$ . The solid curve is corresponds to the decay at  $4.2\text{K}$ . The dot-dashed line and the dashed line correspond to the decay at  $15\text{K}$  for the model I and the model II, respectively.

### 5.3 MICROSCOPIC MODEL OF THE OPTICALLY INDUCED DEFECTS

The defect creation in a-As<sub>2</sub>S<sub>3</sub> is examined briefly in this section although we cannot say definitively because of the broad and featureless signals in the amorphous materials. The mechanism of PL1 fatigue is due to the destruction of PL centers. In amorphous As-Se systems, PL efficiency with band-gap excitation is proportional to the arsenic concentration. This suggests that most of the PL centers in amorphous As-Se systems are associated with As-Se bonds. Also in amorphous As-S systems, it is suggested that most of the PL1 centers are associated with As-S bonds since the PL processes in As-S and As-Se systems are similar to each other.

#### 5.3.1 PL CENTERS IN CRYSTALLINE CHALCOGENIDES

The PL1 is largely Stokes-shifted, which shows that the large lattice relaxation occurs at PL1 centers. In order to understand the PL process in amorphous chalcogenides, we will discuss the photoluminescence process in c-As<sub>2</sub>Se<sub>3</sub>.

According to Ristein and Weiser [1988], and Ristein *et al.* [1989, 1990], the photoluminescence centers in c-As<sub>2</sub>Se<sub>3</sub> are self-trapped excitons. The top of the valence band and the bottom of the conduction band consist of lone pair orbitals of the chalcogen atoms and anti-bonding orbital of As-Se bonds, respectively. The lone pair orbitals of Se1 on the upper layer and on the lower layer in fig. 2.16 are parallel to each other. They strongly interact and split into  $\pi$  and  $\pi^*$  states which, since they are both occupied, prevent formation of a real  $\pi$  bond. Thus, the top of the valence band corresponds to the antibonding states of the  $\pi$  bond. In fact, the band calculation [Tarnow *et al.*, 1986] has shown that most of the charge in the topmost occupied band is distributed around Se1 sites with

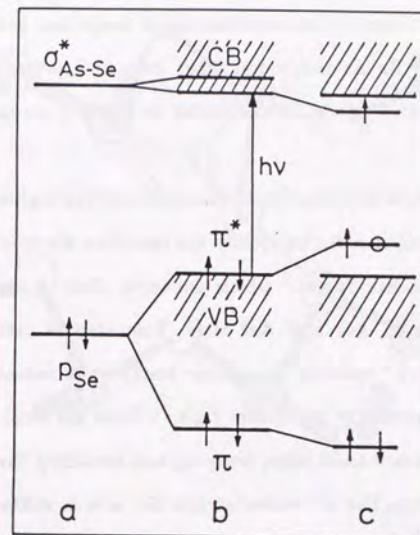


Figure 5.5

Proposed scheme of energy levels involved in the self-trapped exciton in c-As<sub>2</sub>Se<sub>3</sub>. (a) Se1 lone pair state and Se-As antibonding state in non-interacting layers. (b) splitting by interlayer interaction and formation of the highest filled and lowest empty states. (c) After optical excitation and thermalization of the hole a partial  $\pi$  bond is formed, which increases the interlayer splitting of the lone pair band states and reduces the intralayer bond splitting. The  $\pi^*$  and  $\sigma^*$  states move into the gap, localizing the excited carriers. [Ristein and Weiser 1989].

some charge on Se3 but very little contribution from Se2. The interlayer interaction also affects the conduction band states. The charge in the lowest conduction band arising from  $\sigma^*$  states of intralayer bonds has been found to be located too on Se1 and its As neighbours. They have interpreted this as some weakening of the intralayer bonds at this center in favor of stronger interlayer bonding.

A hole created by optical excitation thermalizes into the highest filled states, a  $\pi^*$  state at Se1 sites, thus reducing locally the repulsive electron density. As a consequence Se1 approaches further which enhances their  $\pi$  interaction and weakens their  $\sigma$  bonds to As1 and As2 sites. This step of lattice relaxation increases locally the  $\pi - \pi^*$  splitting (interlayer bond) while reducing the  $\sigma - \sigma^*$  splitting of the strong intralayer bonds (see fig.5.5). Thus the local  $\pi^*$  states are moved up above the valence band edge, trapping and localizing the hole immediately after thermalization. The  $\sigma^*$  states at this Se1 site is shifted down below the conduction band edge due to the reduced  $\sigma - \sigma^*$  splitting of at least one of the As bonds of the Se1 atoms, providing a trap for the electron. Capture of an electron in the antibonding states weakens the As-Se bond, allowing further lattice relaxation. The electron and the hole states move deeper into the gap and form a self trapped exciton states and a radiative center. ODMR measurements confirms this model [Ristein *et al.* 1989, 1990].

### 5.3.2 PL FATIGUE

The similar lattice relaxation process to that in the crystalline chalcogenides may occur at the photoluminescence centers also in the amorphous chalcogenides. In a-As<sub>2</sub>S<sub>3</sub>, the gap states and the tail states of the valence band are formed from the lone pair orbitals of sulfur atoms with interlayer interaction [Watanabe *et al.* 1988]. The interaction may be the  $\pi$ -like interaction, as is the case in the crystalline chalcogenides. The conduction band edge consists

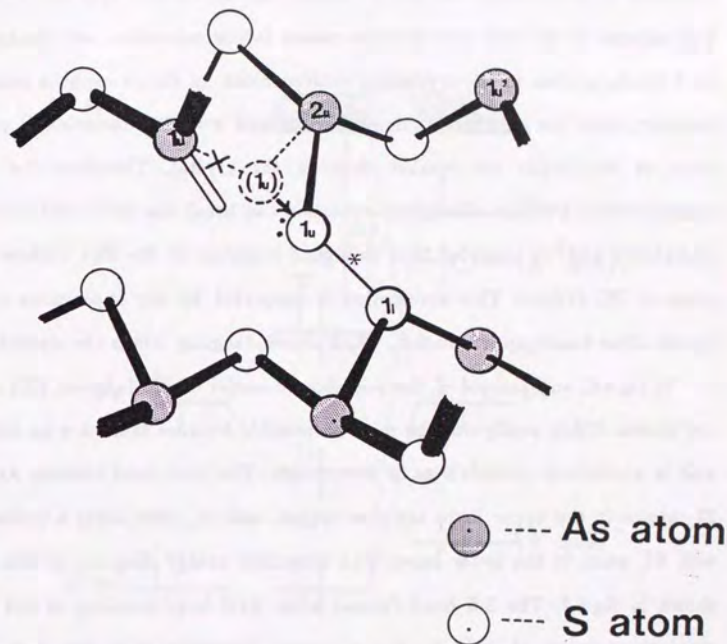


Figure 5.6

The microscopic model of the fatigued PL1 centers. The bond between As1<sub>u</sub> and S1<sub>u</sub> is broken and the ( $\pi$ ) bond between S1<sub>u</sub> and S1<sub>l</sub> is formed.

of the antibonding states of As-S bonds. Thus, the hole generated by optical excitation is thermalized into the  $\pi^*$  states, and an electron into the  $\sigma^*$  states. The capture of the hole and electron causes lattice relaxation and weakens the As-S bonds as does in the crystalline chalcogenides. In the amorphous materials, however, since the structure is more flexible and a lattice distortion is present, some of the bonds are weaker than in the crystal. Therefore the lattice relaxation which occurs after photoexcitation can break the As-S bond with some probability and we consider that this bond-breaking at the PL1 centers is the cause of PL fatigue. This assumption is supported by the appearance of ESR signals after band-gap irradiation, which shows dangling bonds are created.

In fig.5.6, an example of the microscopic model of the fatigued PL1 centers are shown. Other configurations may be possible because there are no structure unit in amorphous materials as in the crystals. The As-S bond between  $As1_u$  and  $S1_u$  atoms in the upper layer are now broken, and  $S1_u$  atom form a  $\pi$ -like bond with  $S1_l$  atom in the lower layer. The schematic energy diagram of this site is shown in fig.5.7. The S-S bond formed after As-S bond breaking is not strong since there is an electron in the  $\pi^*$  state. Therefore it is annealed out at relatively low temperature. Excitation of an electron from  $p_s$  to  $\pi^*$  with below-gap light can break the S-S bond since two electrons occupy the antibonding state, and the bond between  $As1_u$  and  $S1_u$  is reformed, leading to recovery of the PL1 center.

If the electron in the  $\pi^*$  state are removed by, for example, excitation with band-gap light, the S-S bond becomes more stable since there are no electrons in the anti-bonding state. Therefore it is necessary to raise a temperature higher than in the previous case in order to anneal out the fatigued centers. Excitation of an electron from  $p_s$  to  $\pi^*$  state cannot break S-S bond since only one electron occupies the antibonding state. Thus, this model explains the experimental result that the PL1 centers attacked by photoexcitation more than once become the

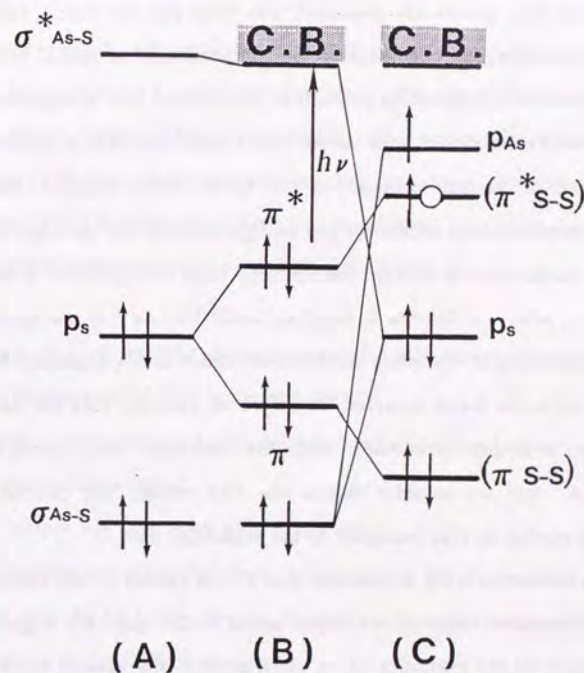


Figure 5.7

Proposed scheme of energy levels involved in the fatigued PL1 center. (A) A lone pair state of sulfur atom and an As-S bonding and antibonding states in non-interacting layers. (B) Splitting by interlayer interaction and formation of the highest filled and lowest empty states. (C) After optical excitation and thermalization of the hole a partial  $\pi$  bond is formed which increases the interlayer splitting of the lone pair band states, reduces the intralayer bond splitting, and finally the As-S bond is broken.

stable fatigued PL centers.

### 5.3.3 PL2 CENTERS

Since the PL2 centers are generated with band-gap irradiation, they are also associated with dangling bonds due to the bond-breaking by optical excitation, as was mentioned in the preceding subsection. In section 5.2, it is suggested that the PL2 centers are associated with As-As bonds since the PL2 is observed in the stoichiometric or As-rich samples but not in the S-rich samples. We examine where the bond-breaking occurs for the configuration of  $-S-As-As-S-$ .

If the As-As bond is broken, the resulting bond configuration is the two sets of  $-S-As\cdot$ , where  $\cdot$  denotes a dangling bond.  $-S-As\cdot$  is not specific to the bond configurations that contain As-As bonds and it is not explained why PL2 is not observed in the S-rich samples. Therefore we consider that the As-S bond is broken by band-gap irradiation and the resulting bond configuration is  $-S-As-As\cdot$  and we consider this is the PL2 center. The process of bond-breaking is similar to that described in the subsection 5.3.2.

In the subsection 5.2.1, it is shown that PL2 is caused by the excitation from extended continuous states to the defect states in the gap. We suggest that the PL2 is caused by the excitation of an electron from the valence band to the As dangling bond. The energy level of As-As bond is located at the top of the valence band edge [Bullet 1976]. A hole created by optical excitation near a PL2 center is thermalized into the As-As bond, and the radiative recombination occurs between the As dangling bond and the homopolar bond. The lattice relaxation, which is shown in fig.5.2, will occur when the As-As bond captures the hole. The energy of the As dangling bond is thought to be 1.4eV from the valence band edge since the intensity of PL2 becomes weak for excitation energies below 1.4eV as can be seen in the PLE spectrum.

## Chapter 6

### Summary and Concluding Remarks

We have studied the optically induced metastable states in  $a-As_2S_3$ , especially those related to photoluminescence. We have found that new photoluminescence centers (PL2) are generated with band-gap irradiation at low temperature, while the photoluminescence that has been reported by many authors so far (PL1) is fatigued by band-gap irradiation.

The obtained results related to the PL2 centers are:

1. The energy level of the PL2 center is located 1.4eV above the valence band edge. The Stokes shift of PL2 is about 0.56eV.
2. For excitation energy above 2.2eV, band-to-band excitation becomes dominant and PL2 gets weakly excited.
3. The PL2 centers are associated with As-As bonds.
4. The PL2 centers are converted from a fraction of the PL1 centers which is associated with As-As bonds, that is, from the component responsible for the pair resonance in the ODMR spectrum.
5. The PL2 centers are different from those of optically induced below-gap absorption, since they have different annealing properties.
6. The PL2 decay consists of the singlet recombination and the triplet recombination.
7. The temperature dependence of PL2 decay can be explained by the activation process from the triplet states to the singlet states. The singlet level is about 2 meV higher than the triplet level.

We have also studied the fatiguing processes of PL1. The obtained results

are:

8. The fatigue is caused by destruction of the PL1 centers, which is due to bond-breaking.
9. The fatigued centers attacked by photons twice or more are not completely bleached by illuminating with below-gap light nor by annealing at temperature lower than room temperature, while those attacked once are bleached by illuminating with below-gap light and by annealing at temperature lower than room temperature. The same mechanism can be applied for the PL2 centers.

We have proposed the microscopic models of the optically induced defects.

10. The PL1 fatigue is caused by breaking an As-S bond. The As-S bond is broken by  $\pi$  interaction between the lone pair orbitals of S atoms.
11. The broken centers are stabilized by removing the electron from the  $\pi^*$  orbital.
12. The PL2 is due to the recombination of an electron on an As dangling bond and a hole thermalized into an As-As bond.

## Appendix

### The Principle of ODMR

Reviews of the optically detected magnetic resonance (ODMR) have been made by Cavenett [1981]. The application of ODMR technique to the amorphous chalcogenides has been done by many authors [Depinna 1982, Tada *et al.* 1984, Robins and Kastner 1984, Ristein *et al.* 1989] since the first observation by Suzuki *et al.* [1979]. The explanation of the ODMR principle described here is mainly after Depinna [1982].

Basically ODMR measurements involves monitoring the effects of paramagnetic resonance on photoluminescence intensity or polarization. The principle of ODMR experiments can be well understood by considering a hypothetical example of its application. We consider the case of a distant electron-hole pair system which is often observed in an amorphous semiconductor. We assume that the spin-orbit interaction is weak for simplicity.

In fig. A-1(a), the Zeeman splitting of the energy levels associated with the distant pair in an external magnetic field are presented. The only selection rule expected to survive in the amorphous state is spin conservation and this will cause the singlet sublevels (2 and 3 in fig.A-1(a)) have shorter recombination lifetime than the triplet sublevels (1 and 4 in fig.A-1(a)). Assuming no spin memory in excitation, the different life times causes the larger population in the triplet sublevels than in the singlet sublevels if the spin relaxation time is longer than the optical recombination time.

Applying microwave of a fixed frequency, resonant spin transfer among the Zeeman levels occurs as shown by the solid arrows in fig.A-1(a). The resonant microwave absorption causes the net population of the triplet sublevels to increase and the effective recombination lifetime becomes short. Thus the PL

intensity is enhanced at the resonant magnetic fields and the ODMR signals are observed (fig.A-1(b)). The resonant magnetic field is determined by the spin Hamiltonian

$$H = g_e \mu_B B m_e + g_h \mu_B B m_h,$$

where  $g_e$  and  $g_h$  are the electron  $g$ -factors,  $\mu_B$  is the Bohr magneton, and  $m_e$  and  $m_h$  are the  $z$ -components of the electron and the hole spin operator and  $B$  is the external magnetic field intensity. Thus the ODMR technique has a powerful advantage of directly associating the ESR information with the related luminescence band.

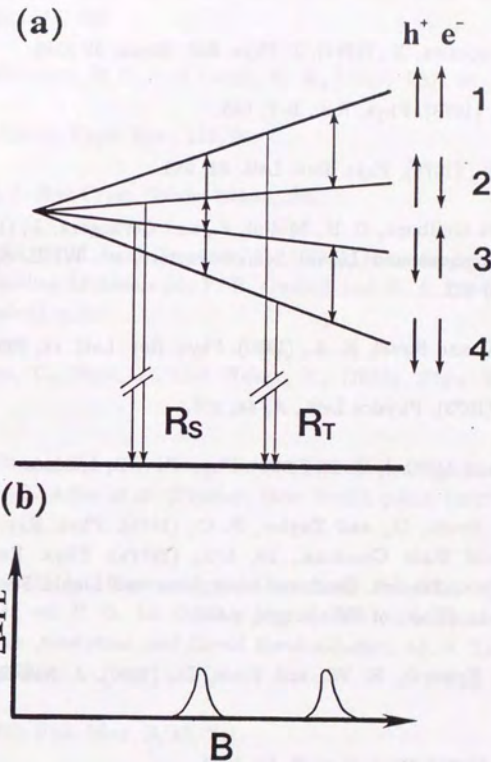


Figure A-1

(a) Zeeman levels of a weakly coupled electron-hole distant pair in an external magnetic field,  $B$ .  $R_S$  and  $R_T$  are the recombination rates for the singlet and triplet sublevels. (b) ODMR signals for such a pair system, corresponding to resonant increases in PL intensity.

## References

- Abe, S. and Toyozawa, Y., (1981). *J. Phys. Soc. Japan*, **50** 2185.
- Agarwal, S. C., (1973). *Phys. Rev. B* **7**, 685.
- Anderson, P. W., (1975). *Phys. Rev. Lett.* **34**, 953.
- Bernoit, C., a la Guillaume, C. B., Mollot, F., and Cernogora, J., (1977). *Proc. Int. Conf. Amorphous and Liquid Semiconductors*, ed. W. E. Spear, (Univ. of Edinburgh) 612.
- Biegelsen, D. K. and Street, R. A., (1980). *Phys. Rev. Lett.* **44**, 803.
- Bishop, S. G., (1973). *Physics Lett., A*, **44**, 107.
- Bishop, S. G. and Mitchel, D. L., (1973). *Phys. Rev. B*, **8**, 5696.
- Bishop, S. G., Strom, U., and Taylor, P. C., (1975). *Phys. Rev. Lett.* **34**, 1346; (1976). *Solid State Commun.*, **18**, 573.; (1977a). *Phys. Rev. B* **15** 2278.; (1977b). *Proc. 7th Int. Conf. on Amorphous and Liquid Semiconductors*, ed W. E. Spear, (Univ. of Edinburgh), p.595.
- Bosch, M. A., Epworth, R. W., and Emin, D., (1980). *J. Non-Cryst. Solids*, **40**, 587.
- Bullet, D. W., (1976). *Phys. Rev. B*, **14**, 1683.
- Cavenett, B. C., (1981)., *Advances in Physics*, **30**, 475.
- Cernogora, J., Mollot, F., and a la Guillaume, C. B., (1973). *Phys. Stat. Sol., A* **15**, 401.; (1974). *Proc. 12th Int. Conf. Physcs os Semiconductors*, ed. M. H. Pilkuhn, p.1027.
- Collins, R. W., Paesler, M. A., and Paul, W., (1980). *Solid State Commun.*, **34**, 833.
- Depinna, S. P., (1982). Thesis, The university of Hull.
- Depinna, S. P. and Cavenett, B. C., (1981). *Solid State Commun.*, **40**, 813; (1982a). *Phys. Rev. Lett.*, **48**, 556; (1982b). *Phil. Mag. B* **46**, 71; (1982c) *Solid State Commun.* **40**, 813.
- Depinna, S. P., Cavenett, B. C., and Lamb, W. E., (1983). *Phil. Mag. B*, **47**, 99.
- De Vore, H. B., (1965), *Phys. Rev.*, **102**, 86.
- Emin, D., (1980). *J. Non-Cryst. Solids*, **35&36**, 969.
- Ewen, R. J. S., Sik, M. J., and Owen, A. E., (1977). *Proceedings of the Structure of Non-Crystalline Materials* ed. P. H. Gaskell and E. A. Davis (Taylor and Francis, London), p.231
- Fischer, R., Heim, U., Stern, F., and Weiser, K., (1971)., *Phys. Rev. Lett.*, **26**, 1182
- Freitas, J. A., Strom, U., and Bishop, S. G., (1985). in *Physics of Disordered Materials* ed. D. Adler *et al.* (Plenum, New York), p.685; (1987). *Phys. Rev. B* **35**, 7780.
- Fritzche, H., (1973). in *Electronic and Structural Properties of Amorphous Semiconductors*, ed. P. G. Le Comber and J. Mort, (Academic, New York) p.55; (1974). in *Amorphous and Liquid Semiconductors*, ed. J. Tauc, (Plenum, New York). p.221.
- Gacizi, P. J., (1982). *Phil. Mag. B*, **45**, 241.
- Gacizi, P. J., and Fritzche, H., (1981). *Soild State Comun.*, **38**, 23.
- Gee, C. M. and Kastner, M., (1980). *J. Non-Crystalline Solids*, **35&36**, 927.
- Hautala, J., Ohlsen, W. D., and Taylor, P. C., (1988). *Phys. Rev. B*, **38**, 11048.
- Hautala, J., Yamasaki, S., and Taylor, P. C., (1989). *J. Non-Cryst. Solids*, **114** 85.
- Higashi, G. S. and Kastner, M., (1981). *Phys. Rev.* **24**, 2295; (1983). *Phil. Mag. B*, **47**, 83.

- Hudgens, H. J., and Kastner, M., (1977). *Proc. of 7th Int. Conf. on Amorphous and Liquid Semiconductors*, ed. W. E. Spear, (Univ. Edinburgh), p.622.
- Kastner, M., Adler, D., and Fritzche, H., (1976). *Phys. Rev. Lett.* **37** 1504.
- Kastner, M., and Hudgens, S. J., (1978). *Phil. Mag. B*, **37**, 665.
- Kawazoe, H., Yanagita, H., Watanabe, Y., and Yamane, M., (1988). *Phys. Rev. B*, **38**, 5661.
- Kolomiets, B. T., Mamontova, T. N., and Babaev, A. A., (1970). *J. Non-Cryst. Solids*, **4**, 289.
- Liu, J. Z., and Taylor, P. C., (1987). *Phys. Rev.*, **59** 1938.
- Lucovsky, G., Galeener, F. L., Geils, R. H., and Keezer, R. C., (1977). *Proceedings of the Structure of Non-Crystalline Materials* ed. P. H. Gaskell and E. A. Davis (Taylor and Francis, London), p.127
- Mollot, F., Cernogora, J., and la' Guillaume, C. B., (1974). *Phys. Stat. Sol., A* **21**, 281.
- Mott, N. F., and Davis, E. A., (1979). *Electronic Process in Noncrystalline Materials*, 2nd edition, Clarendon Press, Oxford)
- Mott, N. F., Davis, E. A., and Street, R. A., (1975). *Phil. Mag.* **32**, 961.
- Murayama, K., and Bosch, M. A., (1981). *Phys. Rev. B*, **23** 6810; (1983). *J. Non-Cryst. Solids*, **59&60** 983.
- Murayama, K. and Ninomiya, T., (1982). *Jpn. J. Appl. Phys.*, **21**, L512.
- Nemanich, R. J., Connell, G. A. N., Hays, T. M., and Street, R. A., (1978). *Phys. Rev. B*, **18** 6900.
- Ngai, K. L., and Murayama, K., (1982). *Physica* **117B & 118B**, 980.
- Owen, A. E. and Robertson, (1970). *J. Non-Cryst. Solids*, **2** 40.
- Ovshinsky, S. R., (1968). *Phys. Rev. Lett.*, **21**, 1450.

- Robins, L. H. and Kastner, M. A., (1984). *Phil. Mag. B*, **50**, 29.; (1987). *Phys. Rev. B* **35**, 2867.
- Ristein, J., and Weiser, G., (1989), *Solid State Commun.* **66**, 361.
- Ristein, J., Taylor, P. C., Ohlsen, W. D., and Weiser, G. (1989). *J. Non-cryst. Solids*, **114**, 91.; (1990) to be published.
- Spear, W. E., and Le Comber, P. G., (1972). *J. Non-Cryst. Solids*, **8-10**, 727.
- Street, R. A., (1976). *Advances in Physics*, **25**, 397; (1978), *Phys. Rev. B*, **17**, 3984; (1984). *Semiconductors and Semimetals 21B*, ed. J. Pancove, (Academec Press, Orlando).
- Street, R. A., and Mott, N. F., (1975). *Phys. Rev. Lett.* **35**, 1293.
- Street, R. A., Searle, T. M., and Austin, I. G., (1973). *J. Phys. C*, **6**, 1830; (1974a). *Phil. Mag.*, **29**, 1157; (1974b). *Ibid.* **30**, 1181; (1975). *Phil. Mag. B*, **32** 431; (1974c). *Amorphous and Liquid Semiconductors*, ed. J. Stuke and W. Bréning (Taylor and Francis, London).
- Street, R. A., Searle, T. M., Austin, I. G., and Sussmann, R. A., (1974d). *J. Phys. C*, **7**, 1582.
- Street, R. A., Austin, I. G., Searle, and T. M., Smith, B. A., (1974). *J. Phys. C*, **7**, 4185; (1974f). *Ibid.* **8**, 1293.
- Strom, U., Freitas, J. A., and Bishop, S. G., (1987). *J. Non-Cryst. Solids*, **97&98**, 1183.
- Suzuki, H., (1982). thesis, Univ. of Tokyo.
- Suzuki, H., Murayama, K., and Ninomiya, T., (1979). *J. Phys. Soc. Japan*, **46**, 693.
- Tada, T., Suzuki, H., Murayama, K., and Ninomiya, T., (1984). *AIP Conference Proceedings No.120, Optical Effects in Amorphous Semiconductors* ed. P. C. Taylor and S. G. Bishop, p.326 (American Institute of Physics, New York).

- Tanaka, Keiji, (1987). Phys. Rev. B, **36**, 9746.
- Tarnow, T., Antonelli, A., and Joannopoulos, J. D., (1986). Phys. Rev. B, **34**, 4059.
- Tauc, J., (1974). *Amorphous and Liquid Semiconductors*, ed. J. Tauc (Plenum Press, London and New York) p.159.
- Toyozawa, Y., (1964). Tech. Rep. ISSP, Ser. A, No. 119.
- Watanabe, Y., Kawazoe, H., and Yamane, M., (1988). Phys. Rev. B, **38**, 5677.
- Wood, D. L., and Tauc, J., (1972). Phys. Rev. **5**, 3144.

